UNIVERSITÄT
BAYREUTH

Masterarbeit

zur Erlangung des akademischen Grades

Master of Science (M. Sc.)

One-body measures of entropy and fundamental measure theory for hard spheres

---

Fakultät für Mathematik, Physik und Informatik

Lehrstuhl Theoretische Physik II

vorgelegt von
Florian Sammüller

Matrikelnummer: 1348208
Kontakt: florian.sammueller@uni-bayreuth.de
Erstgutachter: Prof. Dr. Matthias Schmidt
Zweitgutachter: Prof. Dr. Roland Roth
Bayreuth, 30. März 2020

Zusammenfassung

Um inhomogene Fluide im thermodynamischen Gleichgewicht besser zu charakterisieren und lokale Effekte zu untersuchen, werden zusätzlich zum Dichteprofil $\rho(\mathbf{r})$ weitere Einteilchen-Felder definiert und für das Teilchenmodell harter Kugeln betrachtet. Zunächst wird dafür die lokale Entropiedichte $s(\mathbf{r})$ eingeführt und mittels Monte-Carlo-Simulationen für exemplarische Systeme untersucht. Daraus gewonnene Ergebnisse werden mit den Resultaten einer analytischen Betrachtung verglichen, die den Zusammenhang der Entropiedichte zur Dichtefunktionaltheorie und insbesondere zur fundamentalen Maßtheorie deutlich macht. Neben der Entropiedichte werden die lokale Kompressibilität $\chi_\mu(\mathbf{r})$ und die Entropizität $\chi_T(\mathbf{r})$ als lokale Fluktuationsfelder definiert und Relationen für den Fall harter Kugeln hergeleitet. Es erfolgt ebenfalls eine Untersuchung durch Monte-Carlo-Simulationen für relevante Modellsysteme, in denen fundamentale Eigenschaften dieser neuartigen Einteilchengrößen aufgezeigt und verifiziert werden. Zuletzt wird darauf eingegangen, inwiefern sich die Fluktuationsfelder zur Formulierung eines grundlegenden Minimierungsprinzips eignen.

Abstract

To gain a better understanding of local effects in inhomogeneous fluids at thermodynamic equilibrium, new one-body fields besides the particle density profile $\rho(\mathbf{r})$ are introduced and studied for hard sphere systems. Firstly, the entropy density $s(\mathbf{r})$ is defined and its behaviour in exemplary systems is investigated by Monte-Carlo simulations. An analytic approach, which clarifies the connection of the entropy density to density functional theory and fundamental measure theory, is compared to numerical results and good agreement is found. Secondly, the local compressibility $\chi_\mu(\mathbf{r})$ and the entropicity $\chi_T(\mathbf{r})$ are introduced as local fluctuation profiles and considered again for hard sphere systems. Monte-Carlo simulations are used to explore and verify elementary properties of those new one-body fields. Lastly, the idea of an augmented minimization principle incorporating local fluctuation fields is presented.

Contents

1. Introduction

The description of inhomogeneous fluids is still an important and challenging task in modern theoretical physics as well as in chemistry, biology, material science and numerous other applied fields. Many relevant systems show a variety of phenomena that are particularly hard to tackle. These include e.g. solvation [1], adsorption [2], phase transitions and coexistence [3], mixture of different particle species [4] and even more complex observations like wetting and drying transitions on substrates and interfaces [5–7]. The development of suitable theories describing these phenomena in a generic way has thus been the goal of many physicists for the last decades. Although formalisms of thermodynamics and classical statistical mechanics of many-body systems have become textbook knowledge [8] and provide the tools necessary to answer some of the arising questions in principle, the development of new quantitative and predictive theories that pave the way towards the implementation of efficient numerical algorithms is still of great interest. Furthermore, by deriving new concepts, hitherto unknown simplifications and identities may be discovered.

Of course, much progress has already been made, especially considering computational methods. With molecular dynamics (MD) and Monte-Carlo (MC) simulations becoming more feasible as available computational resources increased, it is now possible to accurately predict the behaviour of many model systems of interest. But although the efficiency of those methods can be improved by various means (Metropolis sampling, umbrella sampling, extended ensemble MC [9], histogram-reweighting [10], transition matrix MC [11], Wang-Landau sampling [12]), the underlying principle is still based on the sampling of a high-dimensional configuration space to obtain estimates for averages of observables.

A framework that drastically reduces the computational cost was established by the development of classical density functional theory (DFT) [13], as it leads the explicit dependence on the distribution function back to one on the particle density $\rho(\mathbf{r})$. A minimization principle can be formulated on the grand potential $\Omega[\rho]$ that, when implemented numerically, is orders of magnitude cheaper than MD or MC routines. However, the difficulty lies in the derivation of this functional for a given internal interaction potential which is the incentive for the considerable amount of work invested in this problem.

For many reasons, the special case of a hard core interaction potential is worth further investigation. Not only can it be considered as a first attempt in stepping away from the ideal gas analytically, there are also numerous practical applications involving a hard core contribution. A common approximation to more complicated interaction potentials is for example the splitting into repulsive and attractive parts [14]. While the latter can be dealt with by a standard mean field treatment, the former are approximated by the already mentioned hard core potential. Due to their central role in the description of inhomogeneous liquids - especially when entropic effects dominate - the main focus of this work will be on systems of hard particles.

Although there has been great success in the application of DFT, some questions still remain – both conceptually and considering practical results. Why is the temperature treated so differently compared to the effective chemical potential? Why are there phenomena like hydrophobicity of substrates and interfaces that seemingly cannot be described well enough with the particle density alone? Why is it so hard to derive density functionals even for simple internal interactions? In this work, light will be shed on some of those questions by considering not only the particle density, but also additional fields.

This thesis is structured as follows. In chapter 2, the definition of a one-body entropy density is presented and applied to equilibrium hard core systems. This new quantity is investigated by Monte-Carlo simulations and the connection to density functional theory is established by the inspection of a common high-accuracy functional for hard particles, derived using fundamental measure theory (FMT). In chapter 3, an alternative but closely related route is taken that leads to the introduction of fluctuation fields which will be called the local chemical susceptibility or local compressibility and the local thermal susceptibility or entropicity. A minimization principle analogous to the one of DFT can be formulated using a set of one-body fields including these local fluctuations. Regarding the usefulness of standard DFT, this property seems very promising for the development of an augmented formulation of functional many-body equilibrium physics. It is therefore investigated both analytically and numerically, how local fluctuations behave in hard particle systems. After concluding the most important aspects of the examined one-body fields in the case of hard core interactions, open questions are discussed and an outlook regarding the generalization of the aforementioned concepts to other particle models and practical applications is given in chapter 4.

2. Entropy density in hard sphere fluids

Albeit not as intuitively comprehensible as other thermodynamic variables, the total entropy S is a key value in the description of many-body physics. In most cases, the constraints that are imposed on a system make S a dependent variable which immediately raises the question how this quantity can be measured or calculated. Especially from a statistical mechanics point of view, it becomes apparent that a determination of the entropy is conceptually difficult since the definition originally attributed to Gibbs and refined by Jaynes [15],

$$S = -k_B \langle \ln \psi \rangle, \tag{2.1}$$

is explicitly dependent on the many-body distribution function ψ. Angled brackets $\langle\cdot\rangle$ denote the average over the suitable thermodynamic ensemble, whereas k_B is Boltzmann's constant. However, the high dimensionality of phase space makes ψ difficult to obtain and the average hard to evaluate analytically.

On the basis of eq. (2.1), a localization to a one-body entropy density $s(\mathbf{r})$, where $\mathbf{r}$ indicates position, is presented and applied to systems of hard particles. MC methods for the determination of $s(\mathbf{r})$ in simulations are developed and the results are compared with a proposed analytic expression for the entropy density of hard spheres derived with FMT.

2.1. Definition and properties of entropy density

2.1.1. Canonical ensemble

By restricting ourselves first to the canonical ensemble with N particles of mass m in D spatial dimensions, we can define the density operator

$$\hat{\rho}_N(\mathbf{r}) = \sum_{i=1}^{N} \delta(\mathbf{r} - \mathbf{r}_i) \tag{2.2}$$

and the canonical trace

$$\mathrm{Tr}_N = \frac{1}{N!\hbar^{DN}} \int \mathrm{d}\mathbf{r}^N \int \mathrm{d}\mathbf{p}^N \tag{2.3}$$

with $\hbar$ being the reduced Planck constant and $(\mathbf{r}^N, \mathbf{p}^N)$ denoting a vector in phase space. The system under consideration has the volume V and is at temperature T. Then the canonical average is given as

$$\langle\cdot\rangle_N = \mathrm{Tr}_N \cdot \psi_N, \tag{2.4}$$

whereby $\psi_N(\mathbf{r}^N, \mathbf{p}^N)$ is the canonical N-body distribution function.

This suggests a definition of the local canonical entropy density by inserting $\hat{\rho}_N(\mathbf{r})/N$ into (2.1):

$$s_N(\mathbf{r}) = -k_B \left\langle \frac{\hat{\rho}_N(\mathbf{r})}{N} \ln \psi_N \right\rangle_N . \tag{2.5}$$

The denominator N is needed for correct normalization as

$$S = \int s(\mathbf{r})\,\mathrm{d}\mathbf{r} \tag{2.6}$$

should hold, which can be proven by exchanging the order of integrations.

With definition (2.5), the entropy density attains the role of a one-body field analogous to the particle density

$$\rho_N(\mathbf{r}) = \langle \hat{\rho}_N(\mathbf{r}) \rangle_N \tag{2.7}$$

that satisfies $N = \int \rho_N(\mathbf{r})\,\mathrm{d}\mathbf{r}$.

Nevertheless, the explicit occurence of the many-body distribution function ψ_N in the canonical average (2.5) is a peculiarity compared to other common one-body fields that emerge from the averaging of microscopic operators. It is beneficial to rewrite this explicit dependence on ψ_N by inserting its known Boltzmann form

$$\psi_N(\mathbf{r}^N, \mathbf{p}^N) = \frac{1}{Z_N} \mathrm{e}^{-\beta H_N(\mathbf{r}^N, \mathbf{p}^N)}, \tag{2.8}$$

whereby Z_N is the canonical partition sum and $\beta = 1/(k_B T)$. Note that we are only considering the equilibrium.

The Hamiltonian of the system is assumed to be of the form

$$H_N(\mathbf{r}^N, \mathbf{p}^N) = \sum_{i=1}^{N} \frac{\mathbf{p}_i^2}{2m} + U_{\mathrm{int}}(\mathbf{r}^N) + \sum_{i=1}^{N} V_{\mathrm{ext}}(\mathbf{r}_i) \tag{2.9}$$

with the one-body external potential $V_{\mathrm{ext}}(\mathbf{r})$ and the interaction energy $U_{\mathrm{int}}(\mathbf{r}^N)$ of a certain configuration $\mathbf{r}^N$.

The insertion of eq. (2.8) into eq. (2.5) yields

$$s_N(\mathbf{r}) = -k_B \left\langle \frac{\hat{\rho}_N(\mathbf{r})}{N} \ln \left(\frac{\exp(-\beta H_N(\mathbf{r}^N, \mathbf{p}^N))}{Z_N} \right) \right\rangle_N \tag{2.10a}$$

$$= -k_B \left\langle \frac{\hat{\rho}_N(\mathbf{r})}{N} \left(\frac{F_N}{k_B T} - \frac{H_N(\mathbf{r}^N, \mathbf{p}^N)}{k_B T} \right) \right\rangle_N \tag{2.10b}$$

$$= -\frac{F_N}{TN} \rho_N(\mathbf{r}) + \frac{1}{TN} \left\langle \hat{\rho}_N(\mathbf{r}) \left(\sum_{i=1}^{N} \frac{\mathbf{p}_i^2}{2m} + U_{\text{int}}(\mathbf{r}^N) + \sum_{i=1}^{N} V_{\text{ext}}(\mathbf{r}_i) \right) \right\rangle_N \tag{2.10c}$$

$$= -\frac{F_N}{TN} \rho_N(\mathbf{r}) + \frac{k_B D}{2} \rho_N(\mathbf{r}) + \frac{\left\langle \hat{\rho}_N(\mathbf{r}) U_{\text{int}}(\mathbf{r}^N) \right\rangle_N}{TN} + \frac{\left\langle \hat{\rho}_N(\mathbf{r}) \sum_{i=1}^{N} V_{\text{ext}}(\mathbf{r}_i) \right\rangle_N}{TN} \tag{2.10d}$$

$$= s_{N,\text{free}}(\mathbf{r}) + s_{N,\text{kin}}(\mathbf{r}) + s_{N,\text{int}}(\mathbf{r}) + s_{N,\text{ext}}(\mathbf{r}). \tag{2.10e}$$

We have identified each contribution with its “physical origin”, namely free energy, kinetic energy, internal interactions and external potential. The latter three terms arise from the explicit insertion of the Hamiltonian (2.9) into (2.10b). In (2.10b), the free energy $F_N = -k_B T \ln Z_N$ was used. The kinetic part was evaluated with the equipartition theorem and the fact that $\langle A(\mathbf{r}^N) B(\mathbf{p}^N) \rangle_N = \langle A(\mathbf{r}^N) \rangle_N \langle B(\mathbf{p}^N) \rangle_N$ for two phase space functions $A(\mathbf{r}^N)$ and $B(\mathbf{p}^N)$ with limited dependence on arguments.

To simplify this expression for hard particle systems, a rewriting of the internal and external part is performed. Note that for hard particles of diameter σ,

$$U_{\text{int}}(\mathbf{r}^N) = \sum_{i=1}^{N} \sum_{j=1, j<i}^{N} \Phi(\mathbf{r}_i, \mathbf{r}_j) \tag{2.11}$$

with the hard core potential

$$\Phi(\mathbf{r}_i, \mathbf{r}_j) = \begin{cases} \infty & |\mathbf{r}_i - \mathbf{r}_j| < \sigma \\ 0 & |\mathbf{r}_i - \mathbf{r}_j| \geq \sigma. \end{cases} \tag{2.12}$$

Therefore, $s_{N,\text{int}}(\mathbf{r})$ vanishes as $U_{\text{int}} = 0$ for all allowed microstates of the system.

The external contribution can be rearranged to

$$s_{N,\text{ext}}(\mathbf{r}) = \frac{1}{TN} \left\langle \hat{\rho}_N(\mathbf{r}) \sum_{i=1}^{N} V_{\text{ext}}(\mathbf{r}_i) \right\rangle_N \tag{2.13a}$$

$$= \frac{1}{TN} \left\langle \hat{\rho}_N(\mathbf{r}) \sum_{i=1}^{N} \int \delta(\mathbf{r}' - \mathbf{r}_i) \, \mathrm{d}\mathbf{r}' V_{\text{ext}}(\mathbf{r}_i) \right\rangle_N \tag{2.13b}$$

$$= \frac{1}{TN} \int \left\langle \hat{\rho}_N(\mathbf{r}) \sum_{i=1}^{N} \delta(\mathbf{r}' - \mathbf{r}_i) V_{\text{ext}}(\mathbf{r}') \right\rangle_N \mathrm{d}\mathbf{r}' \tag{2.13c}$$

$$= \frac{1}{TN} \int \langle \hat{\rho}_N(\mathbf{r}) \hat{\rho}_N(\mathbf{r}') \rangle_N \, V_{\text{ext}}(\mathbf{r}') \, \mathrm{d}\mathbf{r}'. \tag{2.13d}$$

An analogous calculation can be performed for $s_{N,\text{int}}(\mathbf{r})$ in the case of arbitrary pair-interactions and is shown in appendix A.1.

We emphasize that the splitting in eq. (2.10) is not a separation of the dependence on $V_{\text{ext}}(\mathbf{r})$ since the free energy F_N contains information about the external potential as well. Yet, in the canonical case,

$$F_N = F_{N,\text{int}} + \int \rho_N(\mathbf{r}) V_{\text{ext}}(\mathbf{r})\,\mathrm{d}\mathbf{r}, \tag{2.14}$$

which leads to

$$\begin{aligned} s_N(\mathbf{r}) = &-\frac{F_{N,\text{int}}}{TN}\rho_N(\mathbf{r}) + \frac{k_B D}{2}\rho_N(\mathbf{r}) \\ &+ \frac{1}{TN}\int \left(\langle \hat{\rho}_N(\mathbf{r})\hat{\rho}_N(\mathbf{r}')\rangle_N - \rho_N(\mathbf{r})\rho_N(\mathbf{r}')\right) V_{\text{ext}}(\mathbf{r}')\,\mathrm{d}\mathbf{r}'. \end{aligned} \tag{2.15}$$

In eq. (2.15), the last summand contains the influence of the external potential completely.

2.1.2. Grandcanonical ensemble

There are necessary alterations to obtain results in the grandcanonical ensemble, i.e. when the particle number N is not fixed but rather a chemical potential μ is imposed. Grandcanonical trace Tr, average $\langle\cdot\rangle$ and partition sum Ξ are defined as usual:

$$\text{Tr} = \sum_{N=0}^{\infty} \text{Tr}_N, \tag{2.16}$$

$$\langle\cdot\rangle = \text{Tr}\cdot\psi = \sum_{N=0}^{\infty} \text{Tr}_N \cdot \mathrm{e}^{\beta\mu N}\frac{Z_N}{\Xi}\psi_N(\mathbf{r}^N), \tag{2.17}$$

$$\Xi = \sum_{N=0}^{\infty} \mathrm{e}^{\beta\mu N} Z_N. \tag{2.18}$$

The local entropy density

$$s(\mathbf{r}) = -k_B \left\langle \frac{\hat{\rho}_N(\mathbf{r})}{N} \ln\psi \right\rangle \tag{2.19}$$

is then analogous to (2.5) but inherits its grandcanonical nature from the grandcanonical average (that we denote without the subscript N) and the grand ensemble distribution function

$$\psi(\mathbf{r}^N, \mathbf{p}^N) = \frac{1}{\Xi}\mathrm{e}^{-\beta(H(\mathbf{r}^N,\mathbf{p}^N)-\mu N)} = \mathrm{e}^{\beta\mu N}\frac{Z_N}{\Xi}\psi_N(\mathbf{r}^N, \mathbf{p}^N). \tag{2.20}$$

The identification of canonical ψ_N from eq. (2.8) can be obtained by separating $\mathrm{e}^{\beta\mu N}$, the fugacity raised to the power of N, as a prefactor and expanding by Z_N.

We proceed similarly to the canonical case by inserting the equilibrium expression (2.20) of ψ which formally leads to a splitting

$$s(\mathbf{r}) = s_{\text{free}}(\mathbf{r}) + s_{\text{kin}}(\mathbf{r}) + s_{\text{int}}(\mathbf{r}) + s_{\text{ext}}(\mathbf{r}) \tag{2.21}$$

with

$$s_{\text{free}}(\mathbf{r}) = -\frac{\Omega}{T}\left\langle \frac{\rho_N(\mathbf{r})}{N} \right\rangle - \frac{\mu}{T}\rho(\mathbf{r}) = -\frac{1}{T}\left\langle \frac{\rho_N(\mathbf{r})}{N} F_N \right\rangle, \tag{2.22}$$

$$s_{\text{kin}}(\mathbf{r}) = \frac{k_B D}{2}\rho(\mathbf{r}), \tag{2.23}$$

$$s_{\text{int}}(\mathbf{r}) = \frac{1}{T}\left\langle \frac{\hat{\rho}_N(\mathbf{r})}{N} U_{\text{int}}(\mathbf{r}^N) \right\rangle, \tag{2.24}$$

$$s_{\text{ext}}(\mathbf{r}) = \frac{1}{T}\left\langle \frac{\hat{\rho}_N(\mathbf{r})}{N} \sum_{i=1}^{N} V_{\text{ext}}(\mathbf{r}_i) \right\rangle. \tag{2.25}$$

The grand potential $\Omega = -k_B T \ln \Xi$ was identified and the naming conventions of the canonical case have been adopted. Although the Helmholtz free energy is not the appropriate potential in the grandcanonical ensemble, a rearrangement with $F_N = \Omega + \mu N$ still suggests the labeling of $s_{\text{free}}(\mathbf{r})$ that we will thus keep for this contribution. Note however that the actual Helmholtz free energy $F = \Omega + \mu\langle N\rangle$ of the grandcanonical system is obtained by a Legendre transform of the grand potential Ω.

It is straightforward to show that eq. (2.13) holds almost analogously when switching to the grandcanonical average. Different to the canonical case, the factor $1/N$ stays inside of the average so that

$$s_{\text{ext}}(\mathbf{r}) = \frac{1}{T}\int \left\langle \frac{\hat{\rho}_N(\mathbf{r})}{N} \hat{\rho}_N(\mathbf{r}') \right\rangle V_{\text{ext}}(\mathbf{r}')\,\mathrm{d}\mathbf{r}'. \tag{2.26}$$

One has to be cautious of the zero-particle state (i.e. $N = 0$) as it is not well-defined in the formal expression (2.22) of $s_{\text{free}}(\mathbf{r})$. Still, the integral value of this contribution can be evaluated to $1/\Xi$, which leaves the localization of this finite contribution as a choice to be made. An examination of the ideal gas suggests this part to be proportional to the grandcanonical density profile $\rho(\mathbf{r})$. This choice will be applied in the following considerations. The derivations of those two details are presented in appendix A.2.

It seems that a grandcanonical averaging of the splitting (2.10) of the canonical $s_N(\mathbf{r})$ results in the grandcanonical entropy density (2.21)–(2.25). However, in general, there is a discrepancy between the Helmholtz free energy F_N obtained in a canonical N-particle system and $F_N = \Omega + \mu N$ in the grandcanonical version calculated for the same N, which corresponds to no thermodynamic potential. Therefore, although the grandcanonical entropy density relies heavily on canonical information,

$$s(\mathbf{r}) \neq \langle s_N(\mathbf{r})\rangle. \tag{2.27}$$

This can also be proven more directly by recognizing the nonlinearity of its definition (2.19) in the partition function caused by the explicit occurence of $\ln \psi$.

Numerical methods for the computation of $s(\mathbf{r})$ must therefore yield proper grandcanonical information. This will be explored in the next section, where efficient procedures of obtaining $s_N(\mathbf{r})$ or $s(\mathbf{r})$ from simulations are presented.

2.1.3. Numerical methods

The definitions of the local canonical entropy density (2.5) and of its grandcanonical version (2.19) give $s_N(\mathbf{r})$ and $s(\mathbf{r})$ as an explicit average over phase space. However, due to the exponential scaling of the numerical integration w.r.t. its dimensionality, a practical limit is already reached if $ND \approx 4$ for N particles in D spatial dimensions. Therefore, this method is not applicable for complex model systems.

Instead, eq. (2.10) and eq. (2.21) provide means to sample the entropy density in molecular simulations such as MC since all averages and fields are accessible. In most cases (and especially for hard particle systems), standard Metropolis sampling is a reasonable choice. While the sampling of a canonical system is straightforward, there is a variety of methods for the grandcanonical ensemble [16, 17]. In the approach used in this work, each grandcanonical trial move consists of either the insertion of a new particle or the removal or displacement of a randomly chosen one. The displacement trial move is accepted with the common Metropolis probability

$$p_A^{\mathrm{dis}} = \min\left(1, \mathrm{e}^{-\beta\Delta E}\right), \tag{2.28}$$

while the acceptance ratio of insertion and removal is given by [16]

$$p_A^{\mathrm{ins}} = \min\left(1, \frac{V}{\Lambda^3(N+1)}\mathrm{e}^{-\beta\Delta E}\right), \tag{2.29}$$

$$p_A^{\mathrm{rem}} = \min\left(1, \frac{N\Lambda^3}{V}\mathrm{e}^{-\beta\Delta E}\right), \tag{2.30}$$

with the thermal wavelength $\Lambda = \sqrt{2\pi\beta\hbar^2/m}$ and energy difference ΔE of trial and initial configuration.

Solely the thermodynamic potentials F_N in the canonical splitting (2.10) and Ω in eq. (2.22) for the grandcanonical ensemble both pose a difficulty as they cannot be sampled in one conventional Metropolis-MC run. A common procedure to obtain the respective values is thermodynamic integration – the construction of a reversible path from a statepoint with known thermodynamic potential to the one of interest. For hard particles in the canonical ensemble, a suitable path is found by varying the height ϵ of a repulsive step interparticle interaction potential with constant diameter σ. The ideal gas ($\epsilon = 0$) can be used as a reference state and hard core interactions are recovered for $\epsilon \to \infty$.

In the grandcanonical ensemble, a more general approach can be taken by varying the chemical potential μ. Considering the limit

$$\lim_{\mu \to -\infty} \Omega(\mu, V, T) = 0, \tag{2.31}$$

a statepoint with a sufficiently low chemical potential μ_0 provides a suitable reference due to the vanishing grand potential. Hence, for the desired μ,

$$\Omega(\mu, V, T) = \int_{-\infty}^{\mu} \left.\frac{\partial \Omega}{\partial \mu}\right|_{\mu', V, T} \mathrm{d}\mu' \approx \int_{\mu_0}^{\mu} \left.\frac{\partial \Omega}{\partial \mu}\right|_{\mu', V, T} \mathrm{d}\mu' = -\int_{\mu_0}^{\mu} \langle N \rangle|_{\mu', V, T} \, \mathrm{d}\mu', \tag{2.32}$$

where the vertical bar denotes an evaluation with the variables in the subscript. Note that the necessary MC simulations along this path are very efficient since we start from a low density limit and sample only the scalar mean particle number $\langle N \rangle$ for each μ'. Furthermore, this method is independent of the internal interaction potential.

The requirement of reversibility can be limiting and will be discussed in section 3.1. In the considered hard particle systems, no restrictions of this kind occurred and thermodynamic integration was possible.

2.1.4. Monte-Carlo results for hard spheres

It is instructive to apply the methodology of the previous section to some exemplary cases. The results in fig. 2.1 stem from the simulation of a hard sphere system in an external cosine potential of spatial period 6.25σ and amplitude 3ϵ that varies only in the x-direction, i.e.

$$V_{\mathrm{ext}}(x) = 3\epsilon \cos\left(\frac{2\pi x}{6.25\sigma}\right). \tag{2.33}$$

Results for the splitting (2.21) into internal, external, kinetic and free contributions are presented. As already discussed, the internal contribution vanishes due to the hard core nature of the internal potential.

Furthermore, it is interesting to look at the behaviour of $s(\mathbf{r})/\rho(\mathbf{r})$ since fig. 2.1 already suggests a simple connection between $s(\mathbf{r})$ and $\rho(\mathbf{r})$ in some cases. In general, of course, the entropy density is not proportional to $\rho(\mathbf{r})$ as $\langle \hat{\rho}_N(\mathbf{r})/N \rangle \neq \rho(\mathbf{r})/\langle N \rangle$. But in the case of no internal energetic contribution, one is left with terms that are either proportional to $\rho(\mathbf{r})$, to $\langle \hat{\rho}_N(\mathbf{r})/N \rangle$ or to $\langle \hat{\rho}_N(\mathbf{r}) E_{\mathrm{ext}}(\mathbf{r}^N)/N \rangle$, where $E_{\mathrm{ext}}(\mathbf{r}^N)$ denotes the total external energy.

It is observed that in the thermodynamic limit, i.e. for $N \to \infty$, $\langle \hat{\rho}_N(\mathbf{r})/N \rangle \to \rho(\mathbf{r})/\langle N \rangle$ since the distribution of the particle number N,

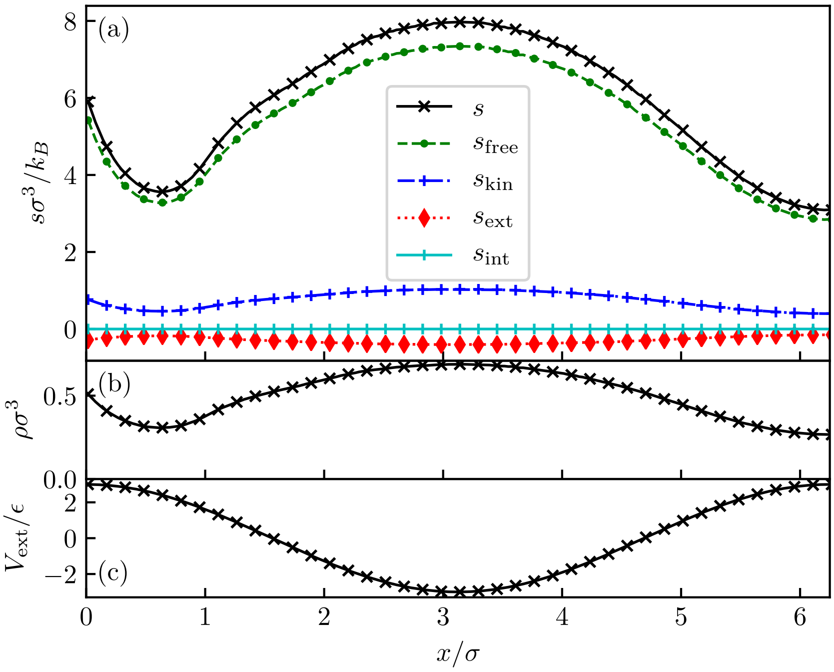

Figure 2.1.: The influence of an external cosine potential in a system at temperature $T = 1.0\epsilon/k_B$ and chemical potential $\mu = -7.0\epsilon$ with planar geometry is shown. Hard spheres are confined between two hard walls at a distance of 12.5σ and periodic boundary conditions in the remaining two directions are applied. Only the left half of the mirror symmetric system is depicted. The wavelength of the external potential (c) was chosen such that two periods fit in the cavity. Due to large external energetic modulation with an amplitude of 3ϵ, the density profile (b) is notably altered to that in the case of vanishing $V_{\rm ext}$. The minimum of $V_{\rm ext}(x)$ at $x \approx 3\sigma$ causes a global maximum of $\rho(x)$, whereas the contact value of the density at the hard wall is reduced. Most importantly, the splitting of $s(x)$ into all parts of eq. (2.21) is shown (a). Trivially, $s_{\rm int}(x) = 0$ due to the hard core nature of interparticle interactions. It is also apparent that $s(x)$ has the same behaviour as $\rho(x)$ since the system is sufficiently large so that correlations of the density operator to global quantities such as the particle number N or the total external energy $E_{\rm ext}$ vanish. The largest contribution to the entropy density is $s_{\rm free}(x)$. Proportionality to $\rho(x)$ for the kinetic part $s_{\rm kin}(x)$ is expected due to eq. (2.23) and indeed observed. The external contribution $s_{\rm ext}(x)$ is small and negative, since the total energy $E_{\rm ext}(\mathbf{r}^N) < 0$ for most relevant configurations $\mathbf{r}^N$.

$$p(N) = \langle \delta_{N(\mathbf{r}^N,\mathbf{p}^N),N} \rangle, \tag{2.34}$$

develops a sharp peak around the mean particle number $\langle N \rangle$. The phase space function $N(\mathbf{r}^N, \mathbf{p}^N)$ counts the particles in the system for a certain point $(\mathbf{r}^N, \mathbf{p}^N)$ in phase space and $\delta_{i,j}$ is the Kronecker delta that yields 0 everywhere except for $i = j$, where it has a value of 1.

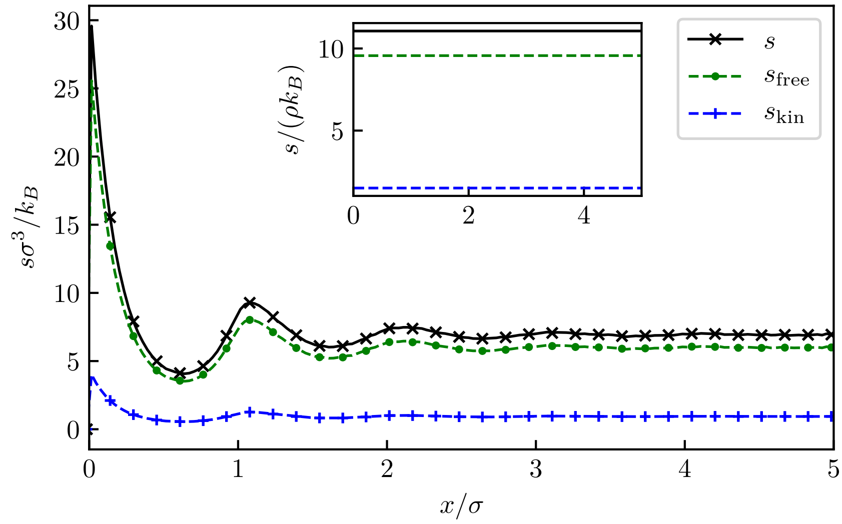

Figure 2.2.: The entropy density in a large system with vanishing external potential becomes proportional to $\rho(x)$. Here, a cavity of length $L = 12.5\sigma$ with hard walls in x-direction and periodic boundary conditions in the remaining two axes was simulated at temperature $T = 1.0\epsilon/k_B$ and chemical potential $\mu = -5.0\epsilon$. The system consists of hard particles of diameter σ and mass $m = 2 * 10^3 \pi \hbar^2/(\epsilon\sigma^2)$. The entropy density profile has a maximum in the vicinity of the hard wall and layering effects are also visible in $s(x)$. The inset shows the ratio $s(x)/\rho(x)$, which is constant throughout the cavity. This also holds for the separate contributions $s_{\text{free}}(x)/\rho(x)$ and $s_{\text{kin}}(x)/\rho(x)$.

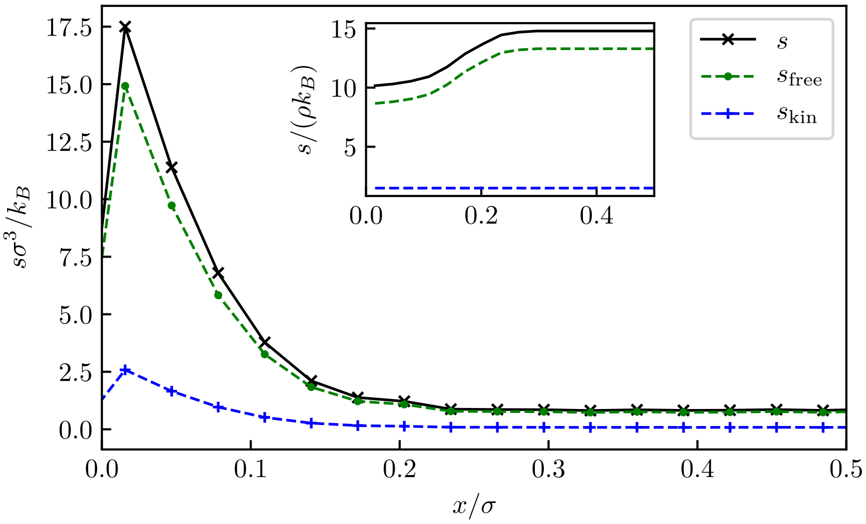

Figure 2.3.: Unlike in fig. 2.2, the entropy density is not proportional to $\rho(x)$ in a narrow hard cubic box of volume $V = (2.0\sigma)^3$. The thermodynamic limit is broken as the relative variance of $p(N)$ is not negligible. The inset shows a non-constant profile of $s(x)/\rho(x)$ and $s_{\text{free}}(x)/\rho(x)$. The kinetic part $s_{\text{kin}}(x)$ is still proportional to $\rho(x)$ due to eq. (2.23). All other parameters are the same as in fig. 2.2.

The configurational energy distribution

$$p(E) = \langle \delta(E_{\text{ext}}(\mathbf{r}^N) - E) \rangle \tag{2.35}$$

for a hard sphere fluid in a large system also degenerates to a delta function at the expectation value $\langle E_{\text{ext}}(\mathbf{r}^N) \rangle$ so that $\hat{\rho}_N(\mathbf{r})$ and $E_{\text{ext}}(\mathbf{r}^N)$ lose their correlation. Under those circumstances, $s(\mathbf{r})/\rho(\mathbf{r})$ becomes constant even in the presence of an external potential. As an illustrative case, we consider hard spheres confined between two hard walls at a sufficiently large distance from each other. Fig. 2.2 displays results from a grandcanonical MC simulation for this case. Notice that $s(\mathbf{r})/\rho(\mathbf{r}) = \text{const.}$ is even true in the vicinity of the hard wall.

We emphasize however that internal interactions and changes to the parameters of the system can alter this result significantly. More precisely, whenever it is not guaranteed that $p(N)$ and $p(E)$ show a sharp peak, the proportionality to the particle density is lost. Therefore, the entropy density stays a relevant nontrivial field. Even in our case of simple hard core interactions, confined systems such as cavities lead to a more complex behaviour as the particle number varies noticeably. This can be seen in fig. 2.3, where the volume of the hard box was reduced to $V = (2.0\sigma)^3$. The ratio $s(\mathbf{r})/\rho(\mathbf{r})$ is not constant in this case, which proves the loss of proportionality.

2.2. Application to classical DFT for hard particles

To demonstrate that the definitions (2.5) and (2.19) are not somewhat arbitrary and of questionable benefit, the profound connection to DFT is shown and a reinterpretation of a common hard sphere functional in the context of the local entropy density is given.

2.2.1. Basic concepts of DFT and FMT

To introduce notation and conventions, a short overview of DFT and FMT is presented. The reader is referred to the pertinent literature for more details [14, 18].

Typically, classical DFT is formulated in the grandcanonical ensemble at chemical potential μ and temperature T. Hence, the central object is the grand potential

$$\Omega([\rho], \mu, T) = F_{\text{int}}([\rho], T) - \int \rho(\mathbf{r})(V_{\text{ext}}(\mathbf{r}) - \mu)\, \mathrm{d}\mathbf{r} \tag{2.36}$$

where $F_{\text{int}}([\rho], T)$ indicates the intrinsic Helmholtz free energy as a density functional independent of $V_{\text{ext}}(\mathbf{r})$. The parametric dependence on T is made explicit here, but will usually be omitted.

A variational principle can be formulated [13], that connects the minimization of $\Omega[\rho]$

w.r.t. $\rho(\mathbf{r})$ to the realized equilibrium density $\rho_0(\mathbf{r})$, i.e.

$$\left.\frac{\delta\Omega[\rho]}{\delta\rho(\mathbf{r})}\right|_{\rho=\rho_0} = 0 \quad (\text{min}). \tag{2.37}$$

A further splitting of the intrinsic Helmholtz free energy functional

$$F_{\text{int}}[\rho] = F_{\text{id}}[\rho] + F_{\text{exc}}[\rho] \tag{2.38}$$

introduces ideal (F_{id}) and excess (F_{exc}) contributions. $F_{\text{id}}[\rho]$ can be derived rigorously, which yields

$$F_{\text{id}}[\rho] = k_B T \int \rho(\mathbf{r}) \Big(\ln(\rho(\mathbf{r})\Lambda^D) - 1\Big)\, \mathrm{d}\mathbf{r}. \tag{2.39}$$

In order to apply DFT to interacting particles, the excess free energy functional has to be specified. The development of suitable approximations of $F_{\text{exc}}[\rho]$ for certain interparticle interactions is still a relevant topic in current literature [19]. Hard particles are a special case since highly accurate functionals can be found due to the purely geometric nature of internal interactions. For hard rods in one spatial dimension, the functional obtained by Percus is even exact [20]. In $D = 3$, the most famous and widely used method is FMT. Thereby, the excess free energy functional is of the form

$$F_{\text{exc}}[\rho] = k_B T \int \Phi(\{n_\alpha(\mathbf{x})\})\, \mathrm{d}\mathbf{x} \tag{2.40}$$

for a one component hard sphere fluid, where $\{n_\alpha : \alpha = 0, 1, 2, 3\}$ is a set of weighted densities obtained by the convolutions

$$n_\alpha(\mathbf{x}) = (\rho * \omega_\alpha)(\mathbf{x}) = \int \rho(\mathbf{x}')\omega_\alpha(\mathbf{x} - \mathbf{x}')\, \mathrm{d}\mathbf{x}'. \tag{2.41}$$

Equivalent representations of the weight functions $\{\omega_\alpha\}$ exist. We use Kierlik and Rosinberg's scalar weight functions [21] given by

$$\omega_3(x) = \Theta(R - x), \tag{2.42}$$

$$\omega_2(x) = \delta(R - x), \tag{2.43}$$

$$\omega_1(x) = \frac{1}{8\pi}\delta'(R - x), \tag{2.44}$$

$$\omega_0(x) = -\frac{1}{8\pi}\delta''(R - x) + \frac{1}{2\pi x}\delta'(R - x). \tag{2.45}$$

The actual form of $\Phi(\{n_\alpha\})$ as a function of weighted densities is still up to debate [22] and depends on the particular derivation and considered approximations. The approach used by Rosenfeld [23] is an ansatz based on dimensional analysis, where remaining coefficients are obtained such that the functional reconstructs the low-density limit exactly and approximates the behaviour at higher densities. Kierlik and Rosinberg adapted the results to their scalar weight functions and obtained

$$\Phi = -n_0 \ln(1 - n_3) + \frac{n_1 n_2}{1 - n_3} + \frac{n_2^3}{24\pi(1 - n_3)^2}. \tag{2.46}$$

There are improved functionals that overcome some existing deficiencies by incorporating accurate equations of state directly in the derivation, such as the so-called White-Bear versions of Roth et al. [24] and Hansen-Goos and Roth [25]. Still, in this work, eq. (2.46) is taken as a starting point similar to Ref. [26].

Due to the multiple convolution integrals that enter eq. (2.40), the ambiguity of the integrand is already seen here and will be exploited when the entropy density is addressed in the next section.

2.2.2. Connection to entropy density

To further motivate the definition of $s(\mathbf{r})$ and to discuss the role of temperature in DFT, a reformulation of the latter is presented, which incorporates the entropy density as a trial field for minimization as it was already stated by Schmidt [26]. In this approach, $s(\mathbf{r})$ is defined equivalently to (2.19) and Levy's constrained search method is applied to the grand potential which is now a functional of both ρ and s. This leads to a splitting

$$\Omega[\rho, s] = E[\rho, s] - T \int s(\mathbf{r})\, \mathrm{d}\mathbf{r} + \int \rho(\mathbf{r})(V_{\mathrm{ext}}(\mathbf{r}) - \mu)\, \mathrm{d}\mathbf{r} \tag{2.47}$$

and shifts the focus from the intrinsic Helmholtz free energy to the internal energy functional $E[\rho, s]$ as the nontrivial object that incorporates excess contributions. The minimization principle (2.37) can be cast into the Euler-Lagrange equations

$$\left.\frac{\delta E[\rho, s]}{\delta \rho(\mathbf{r})}\right|_{\rho=\rho_0, s=s_0} = \mu - V_{\mathrm{ext}}(\mathbf{r}), \tag{2.48}$$

$$\left.\frac{\delta E[\rho, s]}{\delta s(\mathbf{r})}\right|_{\rho=\rho_0, s=s_0} = T, \tag{2.49}$$

which makes clear that T does not only enter as a mere parameter anymore, but also has a direct influence on the conjugate field $s(\mathbf{r})$ in the minimization. The equilibrium profiles $\rho_0(\mathbf{r})$ and $s_0(\mathbf{r})$ represent the realized particle density and entropy density.

Considering hard sphere systems, it is argued that the internal energy functional is of the form [26]

$$E[\rho, s] = \frac{3\pi\hbar^2}{\mathrm{e}^{5/3}m} \int \rho(\mathbf{r})^{5/3} \exp\left(\frac{s(\mathbf{r}) - s_{\mathrm{HS}}([\rho], \mathbf{r})}{3k_B\rho(\mathbf{r})/2}\right) \mathrm{d}\mathbf{r}. \tag{2.50}$$

It is proposed that a suitable choice of $s_{\mathrm{HS}}(\mathbf{r})$ can be derived using the results of FMT, making $s_{\mathrm{HS}}([\rho], \mathbf{r})$ itself a pointwise functional of the density profile. We first consider the case of a hard external potential, so that s_{ext} vanishes. In this totally athermal system, the free energy is given by

$$F = -T \int s(\mathbf{r})\, \mathrm{d}\mathbf{r}. \tag{2.51}$$

The splitting into ideal and excess contribution induces $s(\mathbf{r}) = s_{\mathrm{id}}(\mathbf{r}) + s_{\mathrm{exc}}(\mathbf{r})$, whereby the ideal part can be derived [26] as

$$s_{\mathrm{id}}(\mathbf{r}) = -k_B\rho(\mathbf{r}) \left(\ln(\rho(\mathbf{r})\Lambda^D) - \frac{D}{2} - 1\right). \tag{2.52}$$

Note that eq. (2.52) is a local version of the well-known Sackur-Tetrode equation [27]

$$S_{\mathrm{id}} = -k_B N \left(\ln\left(\frac{N}{V}\Lambda^D\right) - \frac{D}{2} - 1\right) \tag{2.53}$$

for the total entropy S_{id} of an ideal gas.

The excess part of the entropy density must yield an integral value of $-F_{\mathrm{exc}}/T$, which can be approximated by scalar FMT, cf. section 2.2.1. Of course, a unique identification of the integrand $-k_B\Phi(\mathbf{r})$ with $s_{\mathrm{exc}}(\mathbf{r})$ is not possible. However, it is argued that a rearrangement of integrals can be used to separate one of them in a way that is as unbiased as possible [26]. This can also be motivated by the use of diagrammatic methods which provide a formalized framework for the construction of FMT functionals [28]. A more detailed discussion is presented in appendix A.3, where the reordering of integrations is shown explicitly.

The remaining integrand is then a suitable representation of the hard sphere excess entropy density $s_{\mathrm{HS}}(\mathbf{r})$. This reasoning yields

$$s_{\mathrm{exc}}(\mathbf{r}) = s_{\mathrm{HS}}(\mathbf{r}) = -k_B\rho(\mathbf{r}) \sum_{\alpha=0}^{3} \left(\omega_\alpha * \phi_\alpha\right)(\mathbf{r}) \tag{2.54}$$

with

$$\phi_0 = 1 + \left(\frac{1}{n_3} - 1\right) \ln(1 - n_3), \tag{2.55}$$

$$\phi_1 = -\frac{n_2}{n_3} - \frac{n_2}{n_3^2} \ln(1 - n_3), \tag{2.56}$$

$$\phi_2 = \left(\frac{n_2^2}{4\pi n_3^3} - \frac{n_1}{n_3^2}\right)\ln(1-n_3) - \frac{n_1}{n_3} + \frac{n_2^2(2-n_3)}{8\pi n_3^2(1-n_3)}, \tag{2.57}$$

$$\phi_3 = -\left(\frac{n_0}{n_3^2} - \frac{2n_1n_2}{n_3^3} + \frac{n_2^3}{4\pi n_3^4}\right)\ln(1-n_3) - \frac{n_0}{n_3} + \frac{n_1n_2(2-n_3)}{n_3^2(1-n_3)} - \frac{n_2^3(2n_3^2-9n_3+6)}{24\pi n_3^3(1-n_3)^2}, \tag{2.58}$$

as the hard sphere contribution to the entropy density. Here, $\{n_\alpha\}$ is the same set of weighted densities that was defined in eq. (2.41).

2.3. Comparison of entropy density from MC and FMT

In the following section, a computational scheme will be presented that makes the calculation of $s_{\mathrm{HS}}(\mathbf{r})$, both within the FMT approach and from simulations, possible. This provides a tool necessary to compare the obtained theoretical result (2.54) to the real influence of hard sphere interactions on $s(\mathbf{r})$, which are accessible from particle based simulations such as MC.

2.3.1. Computational scheme

The FMT formalism consists of numerous convolutions which can be evaluated efficiently in Fourier space. We mainly follow the procedure of Levesque et al. [29] but make alterations to the treatment of the weight functions $\{\omega_\alpha\}$ for improved accuracy.

For a better understanding, the standard scheme of scalar FMT is presented in fig. 2.4. The convolutions are dealt with by direct fast Fourier transforms (FFT), inverse fast Fourier transforms (iFFT) and multiplications in Fourier space, while $\{\omega_\alpha\}$ is analytically Fourier transformed ($\mathcal{F}$) and sampled in Fourier space in the beginning of the process.

This treatment of the weight functions induces errors in the discrete representation of $\{\omega_\alpha(x)\}$ in direct space. An alternative route is thus used to retain the accuracy needed for a spatially resolved result and is shown schematically in fig. 2.5. A comparison of the weight functions obtained by both methods can be seen in fig. 2.6. The new route yields exact representations, whereas oscillations are induced in the conventional procedure.

In our new method, only ω_2 and ω_3 are implemented on a grid in direct space. Convolutions with ω_0 and ω_1 are treated by partial integration which yields

$$(f*\omega_1)(\mathbf{r}) = \frac{1}{8\pi}\left[(f*a)(\mathbf{r}) - (\nabla f * \mathbf{c})(\mathbf{r})\right], \tag{2.59}$$

$$(f*\omega_0)(\mathbf{r}) = \frac{1}{8\pi}\left[(f*b)(\mathbf{r}) - \sum_{i,j}\left(\mathbf{H}[f]_{ij} * \mathbf{D}_{ij}\right)(\mathbf{r})\right], \tag{2.60}$$

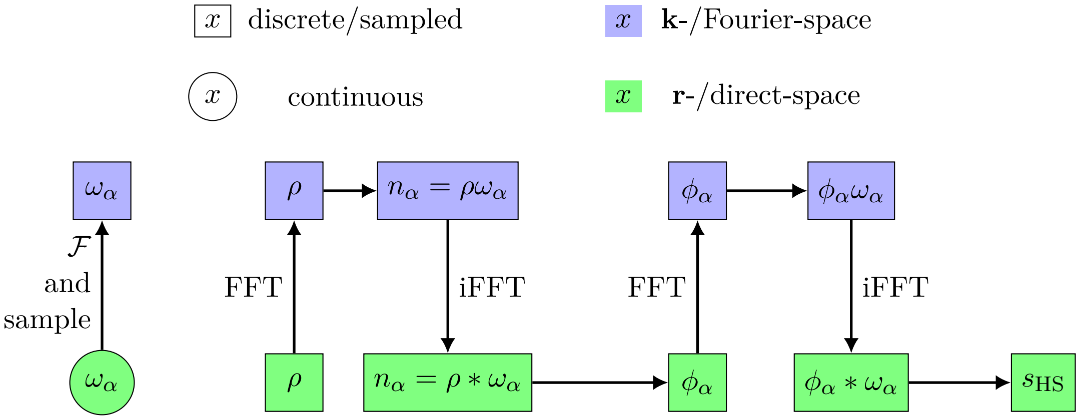

Figure 2.4.: The original scheme of scalar 3D-FMT that is commonly used to get the excess Helmholtz free energy for hard core interactions [29]. Fast Fourier transforms (FFT) and inverse fast Fourier transforms (iFFT) are used to compute the three-dimensional convolutions efficiently by multiplication in **k**-space. The weighted densities $\{\omega_\alpha : \alpha = 0, 1, 2, 3\}$ of eqs. (2.42)–(2.45) are analytically Fourier-transformed ($\mathcal{F}$) and sampled on a grid in **k**-space. We need the spatially resolved quantity $s_{\mathrm{HS}}(\mathbf{r})$ and must have accurate representations of $\{\omega_\alpha\}$ in real space. Therefore, the implementation of weight functions $\{\omega_\alpha\}$ and the evaluation of convolutions is altered and explained in fig. 2.5.

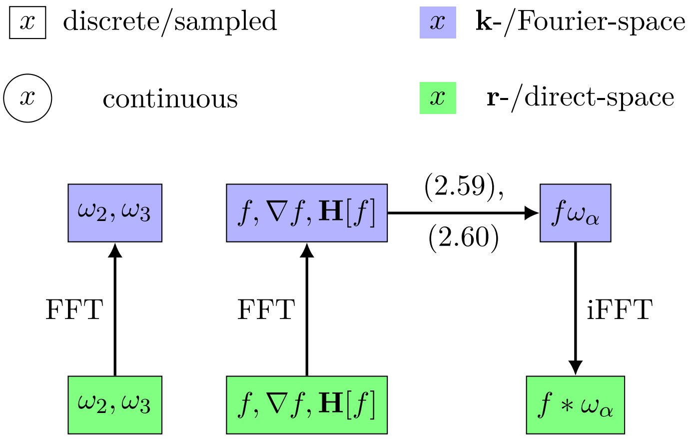

Figure 2.5.: Our improved computational scheme for calculating the convolution of a function f with a weight function. One can see that only ω_2 and ω_3 have to be implemented in real space. The convolutions can be evaluated using f, its gradient ∇f and its Hessian matrix $\mathbf{H}[f]$. For convolutions with ω_1 and ω_0, eqs. (2.59) and (2.60) are applied. This method replaces the original procedure of computing convolutions in fig. 2.4.

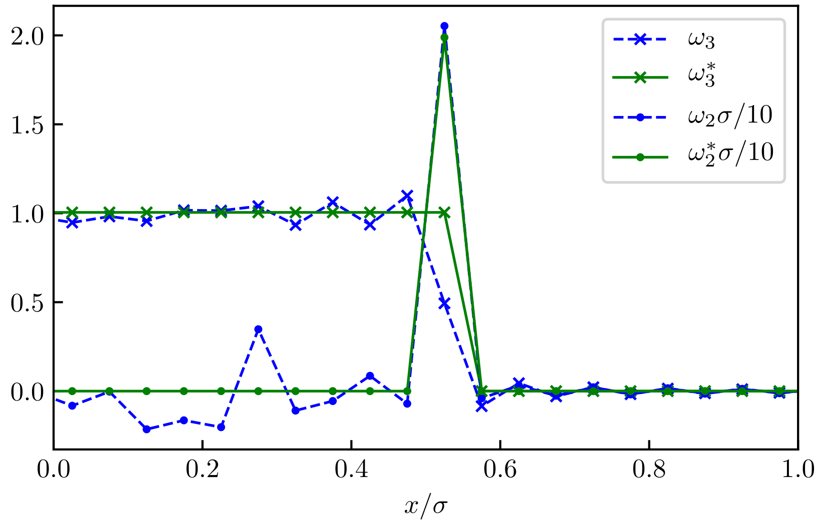

Figure 2.6.: The implementation of $\{\omega_\alpha\}$ in the conventional way induces oscillations in real space. Here, the behaviour of ω_2 and ω_3 is shown (dashed lines). This is compared to our improved method (solid lines, ω_2^*, ω_3^*) which is exact by construction.

for a test function f. In our case, $f = n_\alpha$ or ϕ_α, $\alpha = 0, 1, 2, 3$. The Hessian matrix $\mathbf{H}[f]$ of f is computed with the second-order central-difference scheme and $a, b, \mathbf{c}, \mathbf{D}$ can be evaluated using only ω_2:

$$a(\mathbf{x}) = \frac{2}{x}\omega_2(x), \tag{2.61}$$

$$b(\mathbf{x}) = \frac{2}{x^2}\omega_2(x), \tag{2.62}$$

$$\mathbf{c}(\mathbf{x}) = \mathbf{e_x}\omega_2(x), \tag{2.63}$$

$$\mathbf{D}_{ij}(\mathbf{x}) = (\mathbf{e_x})_i(\mathbf{e_x})_j\omega_2(x). \tag{2.64}$$

With this result, the only weight functions needed for the convolutions are $\omega_2(x) = \delta(R-x)$ and $\omega_3(x) = \Theta(R-x)$. In eqs. (2.63) and (2.64), the unit vector in the direction of $\mathbf{x}$ is denoted by $\mathbf{e_x} = \mathbf{x}/x$.

As a direct comparison, the result of this method is also shown in fig. 2.6 and the improvement is obvious.

2.3.2. Results for hard spheres in a cubic box

With the possibility of an accurate numerical implementation for the FMT framework, a comparison with the aforementioned MC method can be drawn. Thereby, hard spheres of diameter σ and mass $m = 2 \cdot 10^3 \pi\hbar^2/(\epsilon\sigma^2)$ in a three-dimensional cubic box of volume $V = (2.55\sigma)^3$ with hard walls were simulated with the grandcanonical MC scheme of

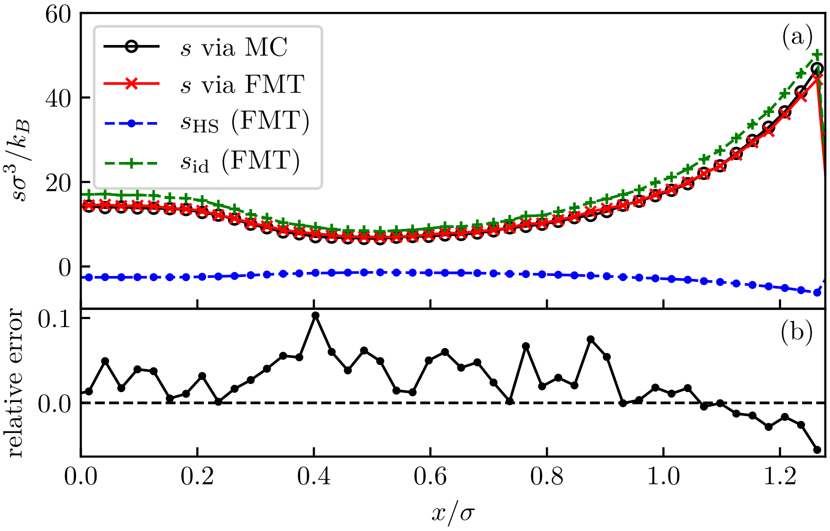

Figure 2.7.: The entropy densities (a) obtained from MC simulation (circles) and from the FMT scheme (crosses) are compared. Also shown is the splitting of s in ideal (s_{id}, pluses) and hard sphere (s_{HS}, dots) contributions. The grandcanonical system under consideration is a three-dimensional cubic hard box of volume $V = (2.55\sigma)^3$ at temperature $T = 1.0\epsilon/k_B$ and chemical potential $\mu = -5.0\epsilon$ containing hard spheres of diameter σ and mass $m = 2 \cdot 10^3 \pi\hbar^2/(\epsilon\sigma^2)$. A slice from the center of the box towards one of its faces is plotted in this figure and is representative for evaluating the agreement of $s(\mathbf{r})$ via MC and $s(\mathbf{r})$ via FMT. A good agreement is observed, which proves that eq. (2.54) is a reasonable approximation to the one-body entropy density for hard sphere systems. The local relative error (b) rarely exceeds 10% and shows that the FMT scheme overestimates the entropy density inside the box but yields lower values than the MC simulation near the walls of the system.

section 2.1.3. Temperature $T = 1.0\epsilon/k_B$ and chemical potential $\mu = -5.0\epsilon$ were imposed and the entropy density $s(\mathbf{r})$ as well as the density profile $\rho(\mathbf{r})$ were obtained. The latter served as a basis for the alternative calculation of $s(\mathbf{r})$ via the FMT route.

The result of both procedures is depicted in fig. 2.7 and good agreement with 5.5% as the root mean square value of the local relative error

$$e(\mathbf{r}) = \frac{s_{\mathrm{FMT}}(\mathbf{r}) - s_{\mathrm{MC}}(\mathbf{r})}{s_{\mathrm{MC}}(\mathbf{r})} \tag{2.65}$$

is found, where $s_{\mathrm{FMT}}(\mathbf{r})$ and $s_{\mathrm{MC}}(\mathbf{r})$ indicate the local entropy density obtained by the FMT and MC method respectively. This error can stem from the noise of the MC simulation, inaccuracy of the thermodynamic integration as well as a systematic deviation of $s_{\mathrm{FMT}}(\mathbf{r})$ from the true entropy density of a hard sphere system. Qualitatively, the FMT scheme underestimates the behaviour of the entropy density near walls but compensates this error by too large values in some inner parts of the box. Therefore, the integral values of $s(\mathbf{r})$ via MC and $s(\mathbf{r})$ via FMT differ only by 0.5%. However, this is expected due to $\int s_{\mathrm{HS}}(\mathbf{r})\,\mathrm{d}\mathbf{r} = -F_{\mathrm{exc}}/T$ and the high accuracy of the conventional FMT functional for F_{exc}.

In conclusion, the FMT framework can not only be used for the determination of functional values for the excess Helmholtz free energy. It was numerically validated that the reordering of integrations performed by Schmidt [26] and explained in appendix A.3 yields an approximate expression for the excess entropy density of a hard sphere system by identifying the integrand of the rearranged free energy functional with $s_{\mathrm{HS}}(\mathbf{r})$. Inversely, the FMT functional can be reinterpreted as a measure that mainly accounts for internal entropic contributions – albeit intricately hidden as convolutions of the density profile.

Of course, the case of a soft external potential still remains for discussion. As already described in section 2.1.4, the entropy density (2.21) in general includes nontrivial correlators that cannot be approximated by the density profile alone. For the case of non-vanishing $s_{\mathrm{ext}}(\mathbf{r})$, this is indeed the case even for a hard sphere system since eq. (2.25) must be taken into account. This means that although the excess entropy density $s_{\mathrm{HS}}(\mathbf{r})$ as a part of $s_{\mathrm{free}}(\mathbf{r})$ can still be evaluated with the FMT framework, the average $\langle \hat{\rho}_N(\mathbf{r}) E_{\mathrm{ext}}(\mathbf{r}^N)\rangle$ is an additional contribution that cannot systematically be formulated as a density functional. Nevertheless, this issue does not alter the interpretation of the FMT functional and the validity of $s_{\mathrm{HS}}(\mathbf{r})$ but shows again that $s(\mathbf{r})$ really is a nontrivial one-body field.

3. Local fluctuations: entropicity and local compressibility

3.1. From entropy density to local fluctuations

In the following chapter, an alternative approach is shown that introduces local one-body fluctuation fields which are closely related to $s(\mathbf{r})$. Although the local entropy density is a well-defined quantity that gives insight to equilibrium properties of entropically driven systems (e.g. consisting of hard particles), its usefulness and accessibility may be limited in some other cases, especially when more realistic particle models are considered.

Certainly, it would be beneficial to avoid the explicit occurence of a thermodynamic potential, since, from a practical point of view, its determination with MC simulations requires additional work. In a system of Lennard-Jones particles for example, one can be faced with phase transitions that make the construction of a reversible path for thermodynamic integration challenging.

On the other hand, it was shown that an additional one-body field such as $s(\mathbf{r})$ can be used to reformulate DFT and is at least approximately accessible for hard particles by common concepts such as FMT. This could be indicative of a more general approach to DFT, which uses not only the density profile $\rho(\mathbf{r})$ but rather multiple variational fields for the minimization of functional values.

Local fluctuation fields, that we call the local thermal susceptibility or entropicity $\chi_T(\mathbf{r})$ and the local chemical susceptibility or local compressibility $\chi_\mu(\mathbf{r})$, are promising candidates for the formulation of a functional minimization principle that augments common classical DFT [30]. In addition, a truly direct sampling of $\chi_T(\mathbf{r})$ and $\chi_\mu(\mathbf{r})$ in molecular simulations is possible and will be applied in section 3.3 for the investigation of hard particle systems. Most importantly, it will be shown that the fluctuation fields themselves attain a physical meaning which is crucial for the interpretation of processes that cannot be explained well enough with the density profile alone. For this reason, the interest in the local compressibility has already grown in current literature over the last few years [31–34]. With our fundamental approach that yields a full set of related fields, we provide further tools to investigate density fluctuations more systematically.

3.2. Theory of local fluctuations

3.2.1. Entropicity and local compressibility

This section summarizes the general results of Eckert et al. [30]. In-depth derivations for the multiple equivalent definitions and the stated relations can be found in Ref. [35].

As a starting point, thermodynamic differentiation of the equilibrium density profile $\rho(\mathbf{r})$ w.r.t. temperature T and chemical potential μ respectively yields

$$\chi_\mu(\mathbf{r}) = \left.\frac{\partial\rho(\mathbf{r})}{\partial\mu}\right|_T, \tag{3.1}$$

$$\chi_T(\mathbf{r}) = \left.\frac{\partial\rho(\mathbf{r})}{\partial T}\right|_\mu. \tag{3.2}$$

Notably, $\chi_\mu(\mathbf{r})$ as introduced by Evans and Stewart [31] is argued by these authors to be of great interest for solvophobicity and hydrophobicity at substrates. In this context, $\chi_T(\mathbf{r})$ can be viewed as a natural extension that complements $\chi_\mu(\mathbf{r})$ and that is worth further investigation.

Another possibility besides the definitions (3.1) and (3.2) of local fluctuations, that reveals a more profound functional structure in the context of inhomogeneous liquids, is the use of functional derivatives as generators of one-body fields. By making use of $\Omega = U - TS - \mu\langle N\rangle$ and $\rho(\mathbf{r}) = \delta\Omega/\delta V_{\text{ext}}(\mathbf{r})|_{\mu,V,T}$, one obtains

$$\chi_\mu(\mathbf{r}) = -\left.\frac{\delta\langle N\rangle}{\delta V_{\text{ext}}(\mathbf{r})}\right|_{\mu,V,T}, \tag{3.3}$$

$$\chi_T(\mathbf{r}) = -\left.\frac{\delta S}{\delta V_{\text{ext}}(\mathbf{r})}\right|_{\mu,V,T}, \tag{3.4}$$

$$\rho^*(\mathbf{r}) = \left.\frac{\delta U}{\delta V_{\text{ext}}(\mathbf{r})}\right|_{\mu,V,T} \tag{3.5}$$

with the response function $\rho^*(\mathbf{r})$ of the total energy U. This also implies that the density profile is composed of those three fluctuation fields, i.e.

$$\rho(\mathbf{r}) = \rho^*(\mathbf{r}) + \mu\chi_\mu(\mathbf{r}) + T\chi_T(\mathbf{r}). \tag{3.6}$$

The one-body field $\rho^*(\mathbf{r})$ can then be interpreted as a local Legendre transform of the density profile $\rho(\mathbf{r})$ due to

$$\rho^*(\mathbf{r}) = \rho(\mathbf{r}) - \mu\frac{\partial\rho(\mathbf{r})}{\partial\mu} - T\frac{\partial\rho(\mathbf{r})}{\partial T}. \tag{3.7}$$

Furthermore, the derivation of correlator expressions is of special interest for numerical implementation in molecular simulations. This is possible for all three fluctuation fields and leads to

$$\begin{aligned}\chi_\mu(\mathbf{r}) &= \langle \beta N \hat{\rho}_N(\mathbf{r})\rangle - \beta\langle N\rangle\rho(\mathbf{r}) \\ &= \operatorname{cov}(\beta N, \hat{\rho}_N(\mathbf{r})),\end{aligned} \tag{3.8}$$

$$\begin{aligned}T\chi_T(\mathbf{r}) &= \langle \beta H \hat{\rho}_N(\mathbf{r})\rangle - \beta\langle H\rangle\rho(\mathbf{r}) - \mu\chi_\mu(\mathbf{r}) \\ &= \operatorname{cov}(\beta H - \beta\mu N, \hat{\rho}_N(\mathbf{r})),\end{aligned} \tag{3.9}$$

$$\begin{aligned}\rho^*(\mathbf{r}) &= \rho(\mathbf{r}) - \langle \beta H \hat{\rho}_N(\mathbf{r})\rangle + \beta\langle H\rangle\rho(\mathbf{r}) \\ &= \rho(\mathbf{r}) - \operatorname{cov}(\beta H, \hat{\rho}_N(\mathbf{r}))\end{aligned} \tag{3.10}$$

with the covariance of two phase space functions A and B defined as $\operatorname{cov}(A,B) = \langle AB\rangle - \langle A\rangle\langle B\rangle$. It is remarkable that no thermodynamic potential occurs on the right hand sides of eqs. (3.8)–(3.10).

In order to split the fluctuation fields into ideal (χ_μ^{id}, χ_T^{id}) and excess contributions (χ_μ^{exc}, χ_T^{exc}), the ideal gas is examined. The analytic results

$$\chi_\mu^{\mathrm{id}}(\mathbf{r}) = \beta\rho(\mathbf{r}), \tag{3.11}$$

$$\chi_T^{\mathrm{id}}(\mathbf{r}) = \frac{1}{T}\left(\frac{D}{2} - \ln(\Lambda^D\rho(\mathbf{r}))\right)\rho(\mathbf{r}) \tag{3.12}$$

for ideal entropicity and local compressibility can be derived and let us define the excess parts as $\chi_\mu^{\mathrm{exc}} = \chi_\mu - \chi_\mu^{\mathrm{id}}$ and $\chi_T^{\mathrm{exc}} = \chi_T - \chi_T^{\mathrm{id}}$.

This allows the formulation of the Ornstein-Zernicke integral equations

$$\chi_\mu^{\mathrm{exc}}(\mathbf{r}) = \rho(\mathbf{r})\int c_2(\mathbf{r},\mathbf{r}')\chi_\mu(\mathbf{r}')\,\mathrm{d}\mathbf{r}', \tag{3.13}$$

$$\chi_T^{\mathrm{exc}}(\mathbf{r}) = \rho(\mathbf{r})\left(\frac{c_1(\mathbf{r})}{T} + \frac{\partial c_1(\mathbf{r})}{\partial T} + \int c_2(\mathbf{r},\mathbf{r}')\chi_T(\mathbf{r}')\,\mathrm{d}\mathbf{r}'\right). \tag{3.14}$$

Thereby, $c_1(\mathbf{r}) = -\delta\beta F_{\mathrm{exc}}/\delta\rho(\mathbf{r})$ and $c_2(\mathbf{r},\mathbf{r}') = \delta c_1(\mathbf{r})/\delta\rho(\mathbf{r}')$ are the one-body and two-body direct correlation function respectively.

The correlator expressions in particular lead to the conclusion that there are similarities to the entropy S and entropy density $s(\mathbf{r})$, especially considering the determination in molecular simulations. If one defines the entropy operator

$$\hat{S} = -k_B\ln\psi, \tag{3.15}$$

the possibility emerges to write the entropicity as the local covariance of the entropy operator with the particle density operator, i.e.

$$k_B T \chi_T(\mathbf{r}) = \mathrm{cov}(\hat{S}, \hat{\rho}_N(\mathbf{r})) = \tilde{s}(\mathbf{r}) - S\rho(\mathbf{r}). \tag{3.16}$$

This can be proven analogously to eq. (2.10) by insertion of the equilibrium distribution function. With the local quantity $\tilde{s}(\mathbf{r}) = -k_B\langle\hat{\rho}_N(\mathbf{r})\ln\psi\rangle$, the connection to the entropy density defined in eqs. (2.5) and (2.19) becomes clear since the expressions differ merely by the factor $1/N$ in the average. Therefore, the correlators needed to reconstruct the fluctuation fields are the same ones as for the entropy density except for the increased order in N. This correspondence also clarifies the term "entropicity" for $\chi_T(\mathbf{r})$, which emphasizes the resemblance to the former entropy density.

There are two major benefits that the local fluctuations possess over the entropy density. Firstly, there is no zero-particle state that needs further attention due to a formal term that is not well-defined for $N = 0$. This could not be prevented for the entropy density in the grandcanonical splitting (2.21). Secondly, the free energy contribution that arises when performing this splitting vanishes due to the difference introduced by the covariance. No thermodynamic integration is needed in this case, which is a significant practical advantage compared to the determination of entropy densities. This means that local fluctuations are readily available in one MC run – even for systems that show complex behaviour such as phase transitions.

3.2.2. Relations for hard particles

The Ornstein-Zernicke equation (3.14) simplifies for hard particles since $\partial c_1(\mathbf{r})/\partial T = 0$ holds. Therefore,

$$\chi_T^{\mathrm{HS}}(\mathbf{r}) = \rho(\mathbf{r})\left(\frac{c_1(\mathbf{r})}{T} + \int c_2(\mathbf{r},\mathbf{r}')\chi_T(\mathbf{r}')\,\mathrm{d}\mathbf{r}'\right). \tag{3.17}$$

Furthermore, due to $\langle U_{\mathrm{int}}\rangle = 0$ and $\langle U_{\mathrm{int}}\hat{\rho}_N(\mathbf{r})\rangle = 0$ in the case of interparticle hard core interactions, the correlator expression for the entropicity reduces to

$$\begin{aligned}
T\chi_T(\mathbf{r}) &= \mathrm{cov}\left(\beta\sum_{i=1}^{N}\left(\frac{p_i^2}{2m} + V_{\mathrm{ext}}(\mathbf{r}_i)\right), \hat{\rho}_N(\mathbf{r})\right) - \mu\chi_\mu(\mathbf{r}) && \text{(3.18a)}\\
&= \frac{D}{2}k_B T\,\mathrm{cov}(\beta N, \hat{\rho}_N(\mathbf{r})) + \mathrm{cov}\left(\beta\sum_{i=1}^{N}V_{\mathrm{ext}}(\mathbf{r}_i), \hat{\rho}_N(\mathbf{r})\right) - \mu\chi_\mu(\mathbf{r}) && \text{(3.18b)}\\
&= \left(\frac{D}{2}k_B T - \mu\right)\chi_\mu(\mathbf{r}) + \mathrm{cov}\left(\beta\sum_{i=1}^{N}V_{\mathrm{ext}}(\mathbf{r}_i), \hat{\rho}_N(\mathbf{r})\right) && \text{(3.18c)}\\
&= \left(\frac{D}{2}k_B T - \mu\right)\chi_\mu(\mathbf{r}) + \beta\int\left(\langle\hat{\rho}_N(\mathbf{r})\hat{\rho}_N(\mathbf{r}')\rangle - \rho(\mathbf{r})\rho(\mathbf{r}')\right)V_{\mathrm{ext}}(\mathbf{r}')\,\mathrm{d}\mathbf{r}' && \text{(3.18d)}\\
&= \left(\frac{D}{2}k_B T - \mu\right)\chi_\mu(\mathbf{r}) + \beta\int H_2(\mathbf{r},\mathbf{r}')V_{\mathrm{ext}}(\mathbf{r}')\,\mathrm{d}\mathbf{r}'. && \text{(3.18e)}
\end{aligned}$$

We used the equipartition theorem for the evaluation of the kinetic part in eq. (3.18a). The same reasoning as in eq. (2.13) leads to the rearrangement in the last line (3.18e) where the two-body density covariance $H_2(\mathbf{r}, \mathbf{r}') = \operatorname{cov}(\hat{\rho}_N(\mathbf{r}), \hat{\rho}_N(\mathbf{r}'))$ occurs. This also shows that although local fluctuations are one-body fields, information about higher-order correlators can be incorporated.

In the case of vanishing external potential $V_{\text{ext}} = 0$,

$$\frac{\chi_T(\mathbf{r})}{\chi_\mu(\mathbf{r})} = \frac{D}{2} k_B - \frac{\mu}{T}, \tag{3.19}$$

which makes the ratio of both fluctuations invariant of position.

Evans and Stewart showed [31] that the local compressibility satisfies the contact theorem

$$\chi_\mu(0^+) = \beta N/V = \beta \rho(\infty) \tag{3.20}$$

at a hard wall potential of the form

$$V_{\text{ext}}(x) = \begin{cases} \infty, & x \leq 0 \\ 0, & x > 0 \end{cases} \tag{3.21}$$

independent of the nature of internal interactions. The argument 0^+ in the contact theorem (3.20) represents a position in the vicinity of the wall whereas ∞ denotes the bulk behaviour far away from it. A similar consideration leads to an analogous contact theorem for the entropicity [36],

$$\chi_T(0^+) = \frac{\beta}{TV}(U - \mu N). \tag{3.22}$$

For the ratio of thermal and chemical wall contact susceptibility, eqs. (3.20) and (3.22) imply that

$$\frac{\chi_T(0^+)}{\chi_\mu(0^+)} = \frac{U}{TN} - \frac{\mu}{T}. \tag{3.23}$$

It is striking that the ratio of those fluctuations obeys a contact theorem that gives an estimate of the internal energy per particle for arbitrary internal interactions.

Keeping in mind that $\chi_T(x)/\chi_\mu(x)$ is spatially homogeneous for hard particles at a hard wall due to eq. (3.19), it immediately follows that the internal energy per particle is constant, as one would expect in that case. Eq. (3.19) is consistent with eq. (3.23) which can again be proven with the equipartition theorem since the kinetic part is the only contribution to the internal energy U in this situation.

The contact theorems (3.20), (3.22) and (3.23) may become of special interest for various interparticle interactions that are not of the hard core type, e.g. Lennard-Jones or

Gaussian particles. Local fluctuations in those particle models were studied in Ref. [36].

3.3. MC results for hard sphere systems

To test the obtained relations described in section 3.2 and to get insight into the behaviour of $\chi_\mu(\mathbf{r})$ and $\chi_T(\mathbf{r})$ in inhomogeneous situations, MC simulations for hard sphere systems are performed. The numerical method is analogous to that described in section 2.1.3 for the sampling of averages in eqs. (3.8), (3.9) and (3.10). Since thermodynamic integration is now avoided and no numerical derivatives – as the definitions (3.1) and (3.2) by thermodynamic derivatives of the density profile would suggest – have to be evaluated, a truly direct sampling in one conventional Metropolis-MC run is possible.

Nevertheless, it is apparent that covariances have a worse signal-to-noise ratio than simpler one-body fields such as $\rho(\mathbf{r})$. This behaviour is due to the generally small difference of $\langle AB\rangle$ and $\langle A\rangle\langle B\rangle$ for two phase space functions A and B. Hence, to obtain acceptable results for $\mathrm{cov}(A, B)$, longer MC runs are needed for the convergence of this small difference.

The computation of $\chi_\mu(\mathbf{r})$ and $\chi_T(\mathbf{r})$ via numerical derivatives of $\rho(\mathbf{r})$ is still possible, of course, and will be applied below as a consistency check. Due to their original definition of $\chi_\mu(\mathbf{r})$ and the application of a DFT scheme, Evans et al. [7] used solely this method for the evaluation of the local compressibility. It was however already recognized that the local compressibility is an indicator for the fluctuation of the liquid density and that it can also be expressed as the correlator term (3.8) [32, 33]. Still, computational advantages of the more direct covariance route will be shown in our context of particle based simulations.

3.3.1. Interpretation of local fluctuations

As before, hard spheres in a confinement of two parallel hard walls and periodic boundary conditions in the remaining directions are simulated. The distance of the walls is chosen sufficiently large so that a mutual influence is avoided. Thus, the simulation serves as an approximation to a bulk fluid in contact with only one wall.

Although the strictly positive density profile is a linear combination of $\chi_T(\mathbf{r})$, $\chi_\mu(\mathbf{r})$ and $\rho^*(\mathbf{r})$, the fluctuation profiles do not have to obey the constraint of positivity separately. In fig. 3.1, $\chi_T(\mathbf{r})$ and $\chi_\mu(\mathbf{r})$ become negative around $x \approx 0.5\sigma$. A similar observation was made by Evans et al. [7] for the local compressibility $\chi_\mu(\mathbf{r})$ in Lennard-Jones liquids near a solvophilic wall. Our result shows, however, that the presence of this effect is not only due to attractive interactions – be it from internal or external contributions. It can already be reconstructed in an athermal situation where only repulsions

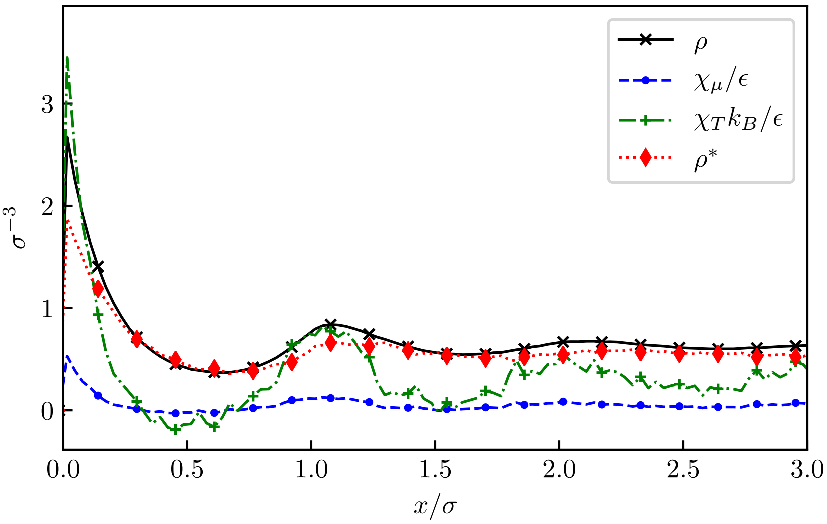

Figure 3.1.: The considered system at $T = 1.0\epsilon/k_B$ and $\mu = -5.0\epsilon$ approximates a hard sphere bulk fluid in contact with a hard wall. Layering near the wall occurs as usual and is observed in all three fluctuation fields. Local maxima and minima coincide approximately for all fluctuations, although small deviations can still be noticed. Interestingly, while $\rho(x) > 0$ is composed of the three fields, $\chi_T(x)$, $\chi_\mu(x)$ and $\rho^*(x)$ do not have to be strictly positive. Here, negative values of $\chi_T(x)$ and $\chi_\mu(x)$ occur at $x \approx 0.5\sigma$.

of a hard core nature exist.

One might find it unusual that the local susceptibilities can change sign. Let us define the corresponding bulk quantities $\chi_\mu^b = \partial\rho^b/\partial\mu$ and $\chi_T^b = \partial\rho^b/\partial T$ with the bulk density $\rho^b = \langle N \rangle/V$. Since $\Omega(\mu)$ is a concave function of the chemical potential μ as a consequence of the second law of thermodynamics [8],

$$\chi_\mu^b = \frac{1}{V}\left.\frac{\partial\langle N\rangle}{\partial\mu}\right|_{V,T} = -\frac{1}{V}\left.\frac{\partial^2\Omega}{\partial\mu^2}\right|_{V,T} > 0. \tag{3.24}$$

As we showed, this property is not true for $\chi_\mu(\mathbf{r})$ at every position $\mathbf{r}$. A strongly modulated or even locally negative susceptibility can be interpreted as a sign of substantial changes in the local structure of the fluid when shifting the thermodynamic statepoint only by a small amount. In the case of the local compressibility $\chi_\mu(\mathbf{r})$, variations of the chemical potential μ on the structure of $\rho(\mathbf{r})$ are considered. This behaviour could be helpful in the indication of layering or prewetting transitions at substrates or interfaces analogous to the already mentioned use as a sign for solvophobicity and hydrophobicity.

The same reasoning applies for the entropicity $\chi_T(\mathbf{r})$, although its bulk counterpart χ_T^b is not necessarily strictly positive (recognize that a similar calculation to eq. (3.24) would yield an off-diagonal element of the Hessian matrix of $\Omega(\mu, T)$ which shows no

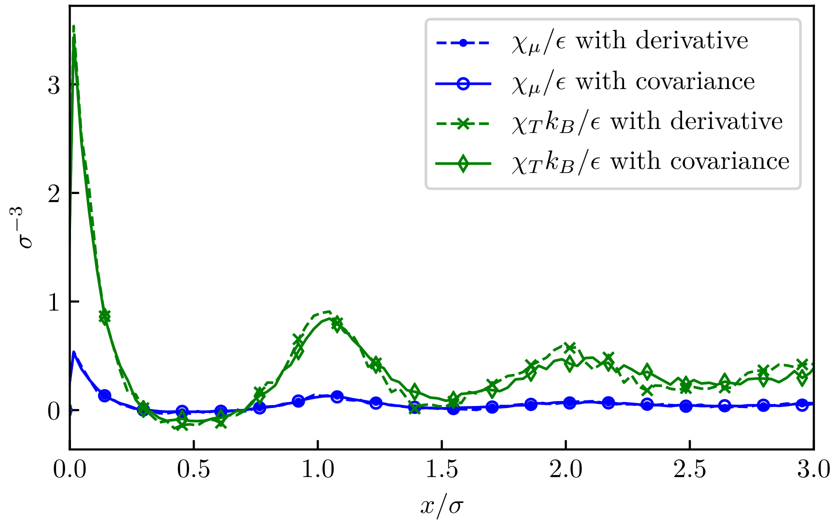

Figure 3.2.: The consistency of definitions (3.1) and (3.2) that make use of derivatives of the density profile and definitions (3.8) and (3.9) that take the covariance route can be verified in this figure. The system in consideration is the same as in fig. 3.1. For the evaluation of numerical derivatives, MC runs of the system at the shifted statepoints $\mu \pm 0.1\epsilon, T \pm 0.02\epsilon/k_B$ were carried out and the central difference was calculated. The individual MC runs are equally long in both cases, but the signal-to-noise ratio is similar in both methods. This shows the numerical difficulty of sampling covariances, although the disadvantage of needing results for multiple thermodynamic statepoints in the case of the derivative route is still prevented.

strict positivity). Still, as the influence of T on the density profile is examined by this quantity, additional information can be gained for systems that show local structural changes due to variations in temperature.

For $\rho^*(\mathbf{r})$, a bulk counterpart is unknown since this field does not emerge directly from a thermodynamic derivative of the density profile. Still, strict positivity is also out of the question as local negative values can already be observed in an ideal gas [35].

In fig. 3.2, the consistency of numerical differentiation and evaluation of covariances is shown. The derivatives are approximated by a central difference, where $\Delta\mu = 0.1\epsilon$ and $\Delta T = 0.02\epsilon/k_B$ around the statepoint $\mu = -5\epsilon$ and $T = 1.0\epsilon/k_B$ are chosen. The agreement proves the equivalence of definitions (3.1) and (3.2) with (3.8) and (3.9) empirically.

Since the considered system is athermal and no energy gauge due to a finite external potential is imposed, the physics of the system only depends on the ratio μ/T. Therefore, the evaluation of both derivatives is redundant, which is also reflected by eq. (3.19) that shows a simple proportionality of $\chi_T(\mathbf{r})$ to $\chi_\mu(\mathbf{r})$. In the following section, this relation is explored further and the influence of a soft external potential on this ratio is investigated.

3.3.2. Thermal vs. chemical susceptibility

We first consider the ratio (3.19) of the susceptibility profiles by simulating the same system as in section 3.3.1. Although eq. (3.19) is exact for hard sphere interactions, the computation of ratios of covariances in MC simulations could induce errors. We show that the covariance route leads to usable results for $\chi_T(\mathbf{r})/\chi_\mu(\mathbf{r})$ that converge even faster than the individual fluctuation profiles.

The result of the MC simulation is shown in fig. 3.3 and the behaviour of the susceptibility ratio is as expected: χ_T/χ_μ does not depend on position and it is constant even in regions where the density profile is strongly modulated due to layering effects near the hard wall. The value of this constant corresponds exactly to the findings of eq. (3.19) since $\chi_T/(k_B\chi_\mu) = 7.5$ for $\mu = -6\epsilon$, $\chi_T/(k_B\chi_\mu) = 9.5$ for $\mu = -8\epsilon$, and $\chi_T/(k_B\chi_\mu) = 11.5$ for $\mu = -10\epsilon$.

In contrast, the situation at a 9-3-Lennard-Jones wall is shown in fig. 3.4 and represents a bulk system in contact with a somewhat soft boundary. Hereby, the external potential

$$V_{\mathrm{ext}}(x) = \begin{cases} \frac{\epsilon}{4}\left[\left(\frac{\sigma}{x}\right)^9 - 3\left(\frac{\sigma}{x}\right)^3 - \left(\frac{\sigma}{x_c}\right)^9 + 3\left(\frac{\sigma}{x_c}\right)^3\right] & x \le x_c \\ 0 & x > x_c \end{cases} \tag{3.25}$$

with the cutoff distance $x_c = 2\sigma$ was chosen.

Layering effects occur as well, but the density profile vanishes continuously in the vicinity of the wall. We expect the ratio $\chi_T(\mathbf{r})/\chi_\mu(\mathbf{r})$ to deviate from the former constant (cf. fig. 3.3) and indeed this is the observed behaviour. Near the wall, the value of the susceptibility ratio increases and follows the structure of the external potential. This behaviour also explains the minimum that occurs in the region $x \approx 1\sigma$, where $V_{\mathrm{ext}}(x)$ has a minimum as well and the particle density peaks. Especially for higher packing fractions, i.e. for larger values of μ, an oscillation that reaches a few hard sphere diameters into the bulk can be seen. Thereby, $\chi_T(\mathbf{r})/\chi_\mu(\mathbf{r})$ behaves inversely to $\rho(\mathbf{r})$ since the former shows local maxima where the latter is relatively small. Therefore, $\chi_T(\mathbf{r})/\chi_\mu(\mathbf{r})$ does not only follow the shape of $V_{\mathrm{ext}}(\mathbf{r})$ directly but also incorporates the effects of internal interactions that transmit the disturbance of the Lennard-Jones wall further into the bulk system. Because of this observation, it is not surprising that this ratio also occurs in the fluctuation functionals which will be introduced in the next section and have to include excess contributions by construction. Physically, $\chi_T(\mathbf{r})/\chi_\mu(\mathbf{r})$ can be viewed as a measure of effective internal energy variations that are imposed on the system by the presence or absence of a virtual test particle at the considered position $\mathbf{r}$. This is seen in the correlator expressions (3.9) and (3.8) since $\chi_T(\mathbf{r})$ incorporates the Hamiltonian of the system and $\chi_\mu(\mathbf{r})$ in the denominator corrects for fluctuations that are purely due

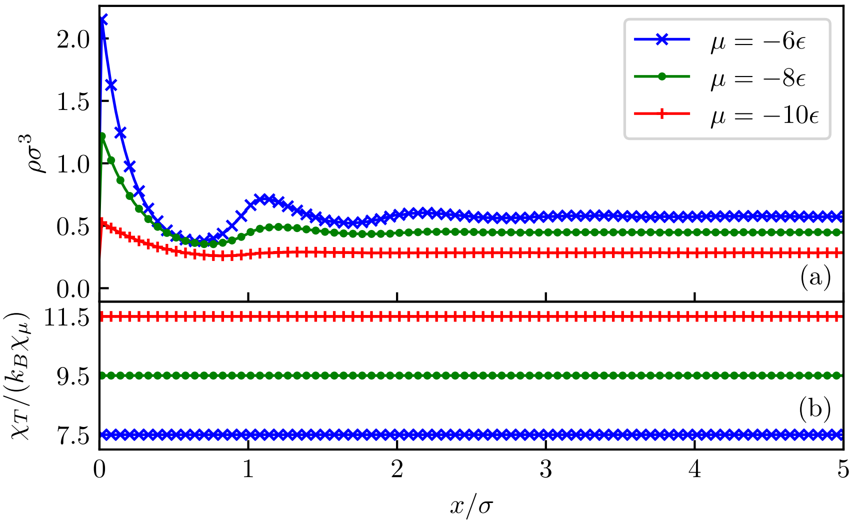

Figure 3.3.: The plot shows (a) the density profile $\rho(x)$ and (b) the susceptibility ratio $\chi_T(x)/\chi_\mu(x)$ of hard particles at a hard wall for various chemical potentials μ and constant temperature $T = 1.0\epsilon/k_B$. Although the structure of $\rho(x)$ changes significantly near the wall, the ratio of $\chi_T(x)$ and $\chi_\mu(x)$ stays constant at a value of $3/2k_B - \mu/T$. This is in agreement with eq. (3.19).

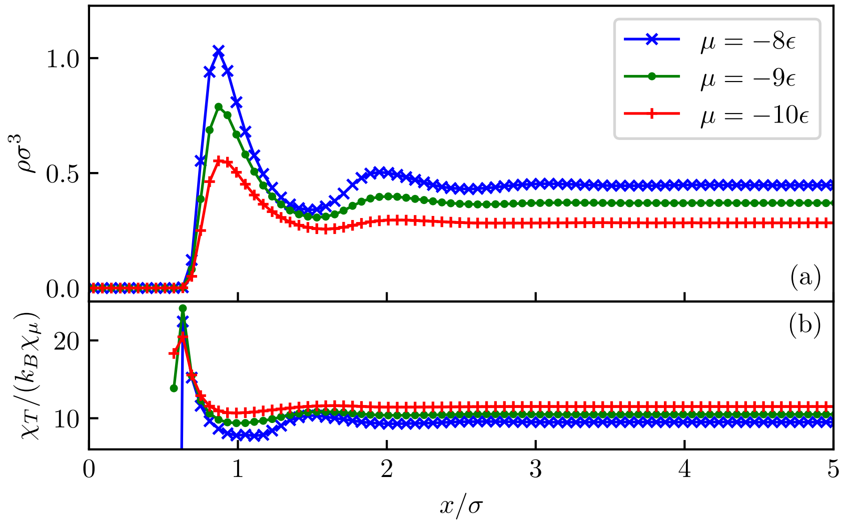

Figure 3.4.: Contrary to fig. 3.19, $\chi_T(\mathbf{r})/\chi_\mu(\mathbf{r})$ at a 9-3-Lennard-Jones wall is not constant and adapts the modulation of $\rho(\mathbf{r})$. An inverse relation is observed, i.e. that the susceptibility ratio (b) is large where the density (a) is low. This coincides with the interpretation of an effective internal energy fluctuation per particle. Far from the wall the behaviour according to eq. (3.19) is recovered.

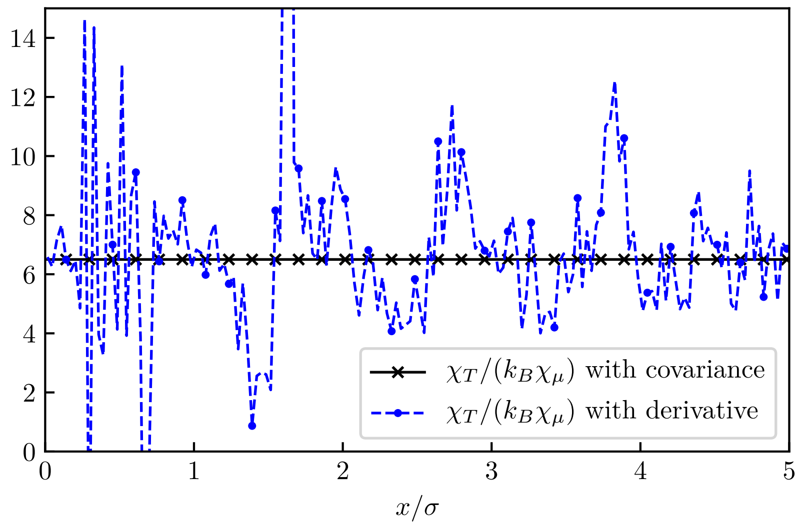

Figure 3.5.: The practical convergence of $\chi_T(\mathbf{r})/\chi_\mu(\mathbf{r})$ in MC simulations can only be guaranteed when avoiding the evaluation of numerical derivatives. With the covariance method (solid line), the noise of both individual fields cancels, while the derivative route (dashed line) leads to the propagation of errors and unusable results. The parameters of the system are those of fig. 3.1.

to variations in particle number.

Numerically, the advantage of the calculation by covariances in one MC run in contrast to the evaluation of numerical derivatives in multiple MC runs at slightly different thermodynamic statepoints becomes apparent when computing the fluctuation ratio $\chi_T(\mathbf{r})/\chi_\mu(\mathbf{r})$. Although the local compressibility $\chi_\mu(\mathbf{r})$ and the entropicity $\chi_T(\mathbf{r})$ individually are equally noisy in both methods (cf. fig. 3.2), since the origin of the noise is the same in the covariance route, the ratio of both quantities retains a much better convergence than the individual fields themselves. This is surprising as we still deal with covariances that are difficult to obtain from MC simulations. But, as one can see, our proficient method leads to the cancellation of errors.

Diametrically opposed to this observation, the derivative route leads to an amplification of errors due to multiple MC runs being used. Fig. 3.5 shows a direct comparison of $\chi_T(\mathbf{r})/\chi_\mu(\mathbf{r})$ obtained by the derivative and the covariance method with MC simulations of equal computational cost. It is apparent that only the latter produces usable results for further calculations.

This is especially important when going beyond the use of fluctuation profiles as individual indicator fields of certain physical processes. For example, if one wants to evaluate the fluctuation functionals that will be presented in the next section, good convergence of the involved terms is crucial for obtaining correct values. Therefore, our computational tools could help in the development of some of the following ideas.

3.4. Minimization principle

One strength of the entropy density of chapter 2 is the possibility to formulate a minimization principle analogous to common DFT that incorporates the density profile $\rho(\mathbf{r})$ as well as the entropy density $s(\mathbf{r})$, cf. section 2.2.2. In the case of fluctuation fields, it is proposed by Eckert et al. that a similar augmentation of DFT is possible, which includes $\rho^*(\mathbf{r})$, $\chi_T(\mathbf{r})$ and $\chi_\mu(\mathbf{r})$ as variational fields of a fluctuation functional $\Gamma[\rho^*, \chi_T, \chi_\mu]$ [30]. Using known results of classical DFT, an argument involving a series of Legendre transforms is applied, which eliminates occurences of $\rho(\mathbf{r})$ and establishes $\Gamma[\rho^*, \chi_T, \chi_\mu]$ as the new central functional. A discussion of this reasoning is illustrated in Ref. [35]. In the following, we summarize the results that were derived in the zero-dimensional limit as a proof of concept.

For the minimization principle, the three Euler-Lagrange equations

$$\left.\frac{\delta\Gamma}{\delta\rho^*(\mathbf{r})}\right|_{\rho_0^*,\chi_{T,0},\chi_{\mu,0}} = -V_{\text{ext}}(\mathbf{r}), \tag{3.26}$$

$$\left.\frac{\delta\Gamma}{\delta\chi_T(\mathbf{r})}\right|_{\rho_0^*,\chi_{T,0},\chi_{\mu,0}} = -TV_{\text{ext}}(\mathbf{r}), \tag{3.27}$$

$$\left.\frac{\delta\Gamma}{\delta\chi_\mu(\mathbf{r})}\right|_{\rho_0^*,\chi_{T,0},\chi_{\mu,0}} = -\mu V_{\text{ext}}(\mathbf{r}) + \frac{V_{\text{ext}}(\mathbf{r})^2}{2} \tag{3.28}$$

can be formulated and are satisfied for the physically realized fluctuation fields $\rho_0^*(\mathbf{r})$, $\chi_{T,0}(\mathbf{r})$ and $\chi_{\mu,0}(\mathbf{r})$. Remarkably, Γ does not depend on temperature T and chemical potential μ.

Analogous to DFT, a splitting of the central functional into ideal and excess part is performed. The ideal gas contribution is evaluated to [30]

$$\Gamma_{\text{id}}[\rho^*, \chi_T, \chi_\mu] = \int \frac{1}{2\chi_\mu(\mathbf{r})} \left[\rho^*(\mathbf{r}) - \exp\left(-\frac{\chi_T(\mathbf{r})}{k_B \chi_\mu(\mathbf{r})}\right)\right]^2 \mathrm{d}\mathbf{r} \tag{3.29}$$

and can be interpreted as a cost functional of fluctuations due to the quadratic structure of the integrand.

As a first approximation to the excess part for hard spheres, we consider the local approximation for the excess free energy on the second virial level, $F_{\text{HS2}} = k_B T \int \rho^2 b/2 \, \mathrm{d}\mathbf{r}$. To lowest order in b [30],

$$\Gamma_{\text{HS2}} = \int \frac{b}{\chi_\mu(\mathbf{r})} \exp\left(-\frac{2\chi_T(\mathbf{r})}{k_B \chi_\mu(\mathbf{r})}\right) \left[\rho^*(\mathbf{r}) - \exp\left(-\frac{\chi_T(\mathbf{r})}{k_B \chi_\mu(\mathbf{r})}\right)\right] \mathrm{d}\mathbf{r}. \tag{3.30}$$

As already mentioned, the presented results follow directly from the scheme of Legendre transforms and are only a first attempt for this kind of generalization. Hence, current work is still invested in a first-principles derivation starting from a many-body object analogous to classical DFT, where the formal proof of the minimization is based on the Mermin grand potential functional

$$\Omega_M[\psi] = \langle \hat{\Omega}_M \rangle_\psi = \mathrm{Tr}\psi\hat{\Omega}_M = \mathrm{Tr}\psi(H - \mu N + k_B T \ln \psi) \tag{3.31}$$

with the Mermin operator $\hat{\Omega}_M$. Eq. (3.31) attains a global minimum for the equilibrium many-body distribution function $\psi(\mathbf{r}^N, \mathbf{p}^N) = \psi_0(\mathbf{r}^N, \mathbf{p}^N)$ and establishes a unique mapping $\rho(\mathbf{r}) \to V_{\mathrm{ext}}(\mathbf{r})$.

Yet, there is a chance that the Mermin grand potential is not the only many-body object that has those desired properties. There are promising candidates for alternative functionals that incorporate

$$\mathrm{var}(\hat{\Omega}_M)_\psi = \mathrm{cov}(\hat{\Omega}_M, \hat{\Omega}_M)_\psi = \langle \hat{\Omega}_M \hat{\Omega}_M \rangle_\psi - \Omega_M^2[\psi] \tag{3.32}$$

and that will be presented in further works. The discovery of a new functional that attains a minimum for ψ_0 and that generates the aforementioned fluctuation profiles in a certain bijective mapping would promote the development of a completely unexplored branch of functional many-body physics.

4. Conclusion and outlook

In this work, we have shown that apart from the density profile $\rho(\mathbf{r})$, further one-body fields are worthy of consideration in statistical and functional many-body mechanics. We first defined the entropy density $s(\mathbf{r})$ as an abstract object that incorporates the many-body distribution function explicitly. With the rewriting of eqs. (2.10) and (2.21), this quantity can be sampled in MC simulations and its behaviour in numerous systems of interest can be studied. Although we focused primarily on hard spheres in cubic or periodic boxes as a rudimentary model of confined inhomogeneous fluids, calculations for arbitrary internal interactions and much more intricate system geometries are achievable and expected to yield interesting results.

As an outlook, $s(\mathbf{r})$ could play an important role in systems that show phase transitions. Generally, in finite systems, where correlations between particle density and total energy or particle number become large, the entropy density should serve as an independent field that may describe physical effects more accurately or concisely than its sole competitor $\rho(\mathbf{r})$. The feasibility of thermodynamic integration as a means to compute the free energy part can be limited, though. However, it should be noted that there are more complex methods of obtaining thermodynamic potentials from MC simulations that were not discussed in this thesis and that could provide a solution to this technical problem [37, 38].

Furthermore, an analytic expression for $s(\mathbf{r})$ in the case of hard spheres was proposed and was shown to lead to a reasonable agreement when compared with MC results. The derivation was based on FMT, which indicates that techniques commonly associated to DFT could be used to obtain this approximation. Vice versa, the agreement lead to the conclusion that the hard sphere density functional can be reinterpreted as effectively incorporating the entropy density. This observation could be important in the development of new functionals, maybe even by rethinking DFT in terms of an internal energy functional depending on both $\rho(\mathbf{r})$ and $s(\mathbf{r})$ as described in section 2.2.1.

Notably, to obtain precise results in the FMT calculation, a state-of-the-art method of 3D-FMT exploiting a computational scheme based on fast Fourier transforms was used. Nevertheless, it needed to be altered to prevent a systematic loss of accuracy for the local excess entropy density. Although such effects are not noticed when evaluating integral values such as F_{exc}, our scheme prevents inaccuracies in the weight functions from the ground up.

It would be interesting to apply the presented framework to mixtures of hard spheres that differ in their diameter. A generalization of the involved functionals and the method of appendix A.3 is straightforward if the distinction of hard sphere species is included. An agreement in this case would further justify the identification of $s_{\mathrm{HS}}(\mathbf{r})$ in the rearranged F_{exc}. More complex particle models of hard core nature such as oblate or prolate spheroids could also be investigated in detail.

Regarding interparticle interactions different from the hard sphere type, it is still an open question whether and if so how analytic approximations to $s_{\mathrm{exc}}(\mathbf{r})$ can be found.

The development of an additional perspective on the derivation of additional one-body fields was motivated in chapter 3, which lead to the introduction of local fluctuation profiles. Those cannot only be seen as simple partial derivatives of the density profile, but also as much more elaborate objects that stem from functional generators, covariances and Ornstein-Zernicke equations.

The behaviour of those fluctuation fields was again studied for hard sphere systems, which already showed that they differ significantly from their bulk counterparts. Some observations of other works, that only considered the local compressibility in a Lennard-Jones fluid and thus incorporated an attractive interaction part, could be recovered in purely athermal hard particle systems.

It is emphasized that our point of view is more general than that of other mentioned works, which only consider the local compressibility $\chi_\mu(\mathbf{r})$ [7, 31–33]. We propose to have a full set of local fluctuation fields that can be derived systematically via multiple routes. While the local compressibility $\chi_\mu(\mathbf{r})$ is already explored, to our knowledge, the local thermal susceptibility or entropicity $\chi_T(\mathbf{r})$ has not been mentioned before. The same applies to the local energy response ρ^*. In a simultaneous work by Stuhlmüller [36], the behaviour of fluctuation fields in systems of Lennard-Jones and Gauss particles is investigated.

With this full set of fluctuations at hand, one can also consider the ratio of local thermal and chemical susceptibility. This has proven to be instructive since the simple relation (3.19) for hard particles and the contact theorem (3.23), that connects this ratio to the inner energy per particle, could be derived. Because the contact theorem still holds for arbitrary internal interactions, an investigation for more realistic particle models could be useful for a better understanding of internal energetic processes in those systems.

As a consequence of our first-principles approach, the local fluctuation fields attain the role of stand-alone observables that are not mere indication fields for certain phenomena such as solvophobicity or drying and wetting transitions. Although it is still of interest to consider e.g. also the entropicity $\chi_T(\mathbf{r})$ in those situations, our goal is the use of fluctuation fields in a general functional formalism. Section 3.4 therefore serves as a review of our first attempts in the development of this idea. Still, further work in this topic is necessary and expected. Nevertheless, the important task of accurately computing fluctuation fields from particle based simulations was established in this work and could serve as a helpful tool in a first-principles development of fluctuation functional theories.

A. Appendix

A.1. Internal entropy density contribution for pair-interactions

We assume pairwise interactions so that eq. (2.11) is valid with an arbitrary but fixed pair-potential $\Phi(\mathbf{r}_i, \mathbf{r}_j)$. Then,

$$
\begin{aligned}
s_{N,\mathrm{int}}(\mathbf{r}) &= \frac{1}{TN} \left\langle \hat{\rho}_N(\mathbf{r}) U_{\mathrm{int}}(\mathbf{r}^N) \right\rangle_N && \text{(A.1a)} \\
&= \frac{1}{TN} \left\langle \hat{\rho}_N(\mathbf{r}) \sum_{i=1}^{N} \sum_{j=1, j<i}^{N} \Phi(\mathbf{r}_i, \mathbf{r}_j) \right\rangle_N && \text{(A.1b)} \\
&= \frac{1}{2TN} \left\langle \hat{\rho}_N(\mathbf{r}) \sum_{i=1}^{N} \sum_{j=1, j\neq i}^{N} \Phi(\mathbf{r}_i, \mathbf{r}_j) \right\rangle_N && \text{(A.1c)} \\
&= \frac{1}{2TN} \left\langle \hat{\rho}_N(\mathbf{r}) \sum_{i=1}^{N} \sum_{j=1, j\neq i}^{N} \int \delta(\mathbf{r}' - \mathbf{r}_i) \,\mathrm{d}\mathbf{r}' \int \delta(\mathbf{r}'' - \mathbf{r}_j) \,\mathrm{d}\mathbf{r}'' \Phi(\mathbf{r}_i, \mathbf{r}_j) \right\rangle_N && \text{(A.1d)} \\
&= \frac{1}{2TN} \iint \left\langle \hat{\rho}_N(\mathbf{r}) \sum_{i=1}^{N} \delta(\mathbf{r}' - \mathbf{r}_i) \sum_{j=1, j\neq i}^{N} \delta(\mathbf{r}'' - \mathbf{r}_j) \right\rangle_N \Phi(\mathbf{r}', \mathbf{r}'') \,\mathrm{d}\mathbf{r}' \,\mathrm{d}\mathbf{r}'' && \text{(A.1e)} \\
&= \frac{1}{2TN} \iint \Bigg(\left\langle \hat{\rho}_N(\mathbf{r}) \sum_{i=1}^{N} \delta(\mathbf{r}' - \mathbf{r}_i) \sum_{j=1}^{N} \delta(\mathbf{r}'' - \mathbf{r}_j) \right\rangle_N \\
&\qquad - \left\langle \hat{\rho}_N(\mathbf{r}) \sum_{i=1}^{N} \delta(\mathbf{r}' - \mathbf{r}_i) \delta(\mathbf{r}'' - \mathbf{r}_i) \right\rangle_N \Bigg) \Phi(\mathbf{r}', \mathbf{r}'') \,\mathrm{d}\mathbf{r}' \,\mathrm{d}\mathbf{r}'' && \text{(A.1f)} \\
&= \frac{1}{2TN} \iint \left(\langle \hat{\rho}_N(\mathbf{r}) \hat{\rho}_N(\mathbf{r}') \hat{\rho}_N(\mathbf{r}'') \rangle_N \right. \\
&\qquad \left. - \langle \hat{\rho}_N(\mathbf{r}) \hat{\rho}_N(\mathbf{r}') \rangle_N \, \delta(\mathbf{r}' - \mathbf{r}'') \right) \Phi(\mathbf{r}', \mathbf{r}'') \,\mathrm{d}\mathbf{r}' \,\mathrm{d}\mathbf{r}''. && \text{(A.1g)}
\end{aligned}
$$

For the grandcanonical version (2.24) of $s_{\mathrm{int}}(\mathbf{r})$, $1/N$ stays inside of the averages. In the same way as in eq. (A.1), one obtains

$$
\begin{aligned}
s_{\mathrm{int}}(\mathbf{r}) = \frac{1}{2T} \iint \Bigg(&\left\langle \frac{\hat{\rho}_N(\mathbf{r})}{N} \hat{\rho}_N(\mathbf{r}') \hat{\rho}_N(\mathbf{r}'') \right\rangle \\
&- \left\langle \frac{\hat{\rho}_N(\mathbf{r})}{N} \hat{\rho}_N(\mathbf{r}') \right\rangle \delta(\mathbf{r}' - \mathbf{r}'') \Bigg) \Phi(\mathbf{r}', \mathbf{r}'') \,\mathrm{d}\mathbf{r}' \,\mathrm{d}\mathbf{r}''. \qquad \text{(A.2)}
\end{aligned}
$$

A.2. Renormalization of entropic zero-particle state

To obtain the total entropy as the correct integral value of the grandcanonical entropy density, the zero-particle contribution must yield a finite integral value. In particular,

$$\begin{aligned}
S &= \int s(\mathbf{r})\,\mathrm{d}\mathbf{r} && \text{(A.3a)}\\
&= -\frac{\Omega}{T}\sum_{N=0}^{\infty} \mathrm{e}^{\beta\mu N}\frac{Z_N}{\Xi}\frac{\int \rho_N(\mathbf{r})\,\mathrm{d}\mathbf{r}}{N} + \left(-\frac{\mu}{T}+\frac{k_B D}{2}\right)\int \rho(\mathbf{r})\,\mathrm{d}\mathbf{r} + \frac{1}{T}\left\langle \frac{\int \rho_N(\mathbf{r})\,\mathrm{d}\mathbf{r}}{N} H_N(\mathbf{r}^N)\right\rangle && \text{(A.3b)}\\
&= -\frac{\Omega}{T} + \left(-\frac{\mu}{T}+\frac{k_B D}{2}\right)\langle N\rangle + \frac{\langle H_N(\mathbf{r}^N)\rangle}{T} && \text{(A.3c)}\\
&= \frac{U-F}{T}. && \text{(A.3d)}
\end{aligned}$$

This thermodynamic relation is only fulfilled if

$$\frac{\int \rho_N(\mathbf{r})\,\mathrm{d}\mathbf{r}}{N} = 1 \quad \text{for } N = 0, 1, 2, \ldots \tag{A.4}$$

is chosen in (A.3b), which renormalizes the case $N = 0$. Then,

$$\mathrm{e}^{\beta\mu N}\frac{Z_N}{\Xi}\frac{\int \rho_N(\mathbf{r})\,\mathrm{d}\mathbf{r}}{N} = \frac{1}{\Xi} \quad \text{for } N = 0. \tag{A.5}$$

It might be counterintuitive that the zero-particle state gives a non-zero contribution to the total entropy in the grandcanonical ensemble. Of course, in the canonical ensemble, the entropy of an empty system is zero. However, in the grandcanonical ensemble, the particle number is not fixed. Thinking along the lines of Shannon-entropy [39], one can recognize that not knowing the current N leads to a higher information content and thus to a higher entropy per definition. Not the intrinsic properties of the zero-particle state increase the entropy – it is much more the uncertainty if particles are even in the system that leads to this additional contribution.

We now propose a localization of this integral value. In an ideal gas, the canonical density is given by

$$\rho_N(\mathbf{r}) = N\frac{\exp(-\beta V_{\text{ext}}(\mathbf{r}))}{\int \exp(-\beta V_{\text{ext}}(\mathbf{r}'))\,\mathrm{d}\mathbf{r}'}. \tag{A.6}$$

Therefore,

$$\frac{\rho_N(\mathbf{r})}{N} = \frac{\exp(-\beta V_{\text{ext}}(\mathbf{r}))}{\int \exp(-\beta V_{\text{ext}}(\mathbf{r}'))\,\mathrm{d}\mathbf{r}'} = \rho_1(\mathbf{r}), \tag{A.7}$$

which is obvious for $N \neq 0$, but implies a choice for $N = 0$. This choice yields

$$\left\langle \frac{\rho_N(\mathbf{r})}{N} \right\rangle = \sum_{N=0}^{\infty} \mathrm{e}^{\beta\mu N} \frac{Z_N}{\Xi} \frac{\rho_N(\mathbf{r})}{N} = \rho_1(\mathbf{r}) \sum_{N=0}^{\infty} \frac{\mathrm{e}^{\beta\mu N}}{N!} \frac{Z_1^N}{\Xi} \tag{A.8}$$

for the grandcanonical average, where we used the relation $Z_N = Z_1^N/N!$ for the canonical partition sum of the N-body ideal gas with the canonical partition sum Z_1 of an ideal single-particle system.

The grandcanonical density

$$\rho(\mathbf{r}) = \Lambda^{-D} \mathrm{e}^{\beta\mu} \mathrm{e}^{-\beta V_{\text{ext}}(\mathbf{r})} \tag{A.9}$$

and partition sum

$$\Xi = \sum_{N=0}^{\infty} \frac{\mathrm{e}^{\beta\mu N}}{N!} Z_1^N \tag{A.10}$$

of the ideal gas let us identify

$$\left\langle \frac{\rho_N(\mathbf{r})}{N} \right\rangle = \rho_1(\mathbf{r}) = \rho(\mathbf{r})\mathrm{e}^{-\beta\mu} \frac{\Lambda^D}{\int \exp(-\beta V_{\text{ext}}(\mathbf{r}'))\,\mathrm{d}\mathbf{r}'} = \rho(\mathbf{r})\mathrm{e}^{-\beta\mu} Z_1^{-1} = \tag{A.11a}$$

$$= \rho(\mathbf{r}) \left[\frac{1}{\Xi} \mathrm{e}^{\beta\mu} Z_1 \sum_{N=0}^{\infty} \frac{\left(\mathrm{e}^{\beta\mu} Z_1\right)^N}{N!} \right]^{-1} = \tag{A.11b}$$

$$= \rho(\mathbf{r}) \left[\frac{1}{\Xi} \sum_{N=0}^{\infty} \frac{\left(\mathrm{e}^{\beta\mu} Z_1\right)^{N+1}}{N!} \right]^{-1} = \tag{A.11c}$$

$$= \rho(\mathbf{r}) \left[\frac{1}{\Xi} \sum_{N=0}^{\infty} \frac{\left(\mathrm{e}^{\beta\mu} Z_1\right)^{N+1}}{(N+1)!} (N+1) \right]^{-1} = \tag{A.11d}$$

$$= \rho(\mathbf{r}) \left[\frac{1}{\Xi} \sum_{N=1}^{\infty} \frac{\left(\mathrm{e}^{\beta\mu} Z_1\right)^{N}}{N!} N \right]^{-1} = \tag{A.11e}$$

$$= \rho(\mathbf{r}) \left[\frac{1}{\Xi} \sum_{N=0}^{\infty} \frac{\mathrm{e}^{\beta\mu N} Z_1^N}{N!} N \right]^{-1} = \frac{\rho(\mathbf{r})}{\langle N \rangle}. \tag{A.11f}$$

The zero-particle contribution to $s(\mathbf{r})$ is hence chosen to be proportional to the grandcanonical density profile $\rho(\mathbf{r})$. This choice is exact for the ideal gas, but is taken as a reasonable approximation otherwise since the zero-particle state becomes especially important when internal interactions are sparse.

In grandcanonical MC simulations, $\langle \rho_N(\mathbf{r})/N \rangle$ is then ordinarily sampled for $N \geq 1$. Additionally, the number n_0 of occurences of $N = 0$ is counted so that a contribution proportional to $\rho(\mathbf{r})/\langle N \rangle$ can be added with the correct weight n_0/n_s. n_s denotes the total number of samples that contribute to the average.

A.3. Excess entropy density from FMT

FMT for a one-species hard sphere system can be formulated in a power series [28]

$$\mathbf{F}_{\mathrm{exc}} = k_B T \int \sum_{m=2}^{\infty} \frac{1}{m(m-1)} \mathbf{N}(\mathbf{x})^m \, \mathrm{d}\mathbf{x} \tag{A.12}$$

with

$$\mathbf{N} = \begin{pmatrix} n_3 & n_2 & n_1 & n_0 \\ 0 & n_3 & n_2/(4\pi) & n_1 \\ 0 & 0 & n_3 & n_2 \\ 0 & 0 & 0 & n_3 \end{pmatrix}. \tag{A.13}$$

The actual excess free energy then corresponds to the entry in the first row and last column of the matrix $\mathbf{F}_{\mathrm{exc}}$, i.e. $F_{\mathrm{exc}} = (\mathbf{F}_{\mathrm{exc}})_{03}$ if the index range is $\{0, 1, 2, 3\}$. An explicit summation of the series is possible and results in the Kierlik-Rosinberg integrand (2.46).

It is clear that $\mathbf{x}$ is merely an integration variable that does not represent particle positions. But due to definition (2.19) of the entropy density, it is expected that a particle is actually located at a considered position $\mathbf{r}$. Therefore, we single out one $\mathbf{N}(\mathbf{x})$ from the sum, apply its definition

$$\mathbf{N}(\mathbf{x}) = \int \mathbf{W}(\mathbf{x} - \mathbf{r}) \rho(\mathbf{r}) \, \mathrm{d}\mathbf{r} \tag{A.14}$$

with the matrix

$$\mathbf{W} = \begin{pmatrix} \omega_3 & \omega_2 & \omega_1 & \omega_0 \\ 0 & \omega_3 & \omega_2/(4\pi) & \omega_1 \\ 0 & 0 & \omega_3 & \omega_2 \\ 0 & 0 & 0 & \omega_2 \end{pmatrix} \tag{A.15}$$

of Kierlik-Rosinberg weight functions (2.42)–(2.45) and rearrange the order of integrations. This procedure yields

$$\mathbf{F}_{\mathrm{exc}} = k_B T \int \rho(\mathbf{r}) \int \mathbf{W}(\mathbf{x} - \mathbf{r}) \sum_{m=2}^{\infty} \frac{1}{m(m-1)} \mathbf{N}(\mathbf{x})^{m-1} \, \mathrm{d}\mathbf{x} \, \mathrm{d}\mathbf{r}. \tag{A.16}$$

The series over m can be evaluated to a closed-form expression and provides a matrix

$$\mathbf{A} = \begin{pmatrix} a_{00} & a_{01} & a_{02} & \phi_3 \\ a_{10} & a_{11} & a_{12} & \phi_2 \\ a_{20} & a_{21} & a_{22} & \phi_1 \\ a_{30} & a_{31} & a_{32} & \phi_0 \end{pmatrix} \tag{A.17}$$

where solely the last column consisting of the terms (2.55)–(2.58) is relevant (recall that we are only interested in the top right element of $\mathbf{F}_{\text{exc}}$).

Finally,

$$F_{\text{exc}} = k_B T \int \rho(\mathbf{r}) \sum_{\alpha=0}^{3} \left(\omega_\alpha * \phi_\alpha\right)(\mathbf{r})\, \mathrm{d}\mathbf{r} \tag{A.18}$$

follows and $s_{\text{HS}}(\mathbf{r})$ can be identified in accordance with eq. (2.54).

Bibliography

[1]T. Lazaridis, The Journal of Physical Chemistry B **102**, 3531–3541 (1998).

[2]Y.-X. Yu, The Journal of Chemical Physics **131**, 024704 (2009).

[3]R. Evans, Journal of Physics: Condensed Matter **2**, 8989–9007 (1990).

[4]M. Schmidt, H. Löwen, J. M. Brader, and R. Evans, Physical Review Letters **85**, 1934–1937 (2000).

[5]E. Velasco and P. Tarazona, The Journal of Chemical Physics **91**, 7916–7924 (1989).

[6]S. Singh, J. Houston, F. van Swol, and C. J. Brinker, Nature **442**, 526–526 (2006).

[7]R. Evans, M. C. Stewart, and N. B. Wilding, The Journal of Chemical Physics **147**, 044701 (2017).

[8]J.-P. Hansen and I. R. McDonald, *Theory of Simple Liquids* (Elsevier, 2013).

[9]Y. Iba, International Journal of Modern Physics C **12**, 623–656 (2001).

[10]J. J. Potoff and A. Z. Panagiotopoulos, The Journal of Chemical Physics **112**, 6411–6415 (2000).

[11]J. R. Errington, The Journal of Chemical Physics **118**, 9915–9925 (2003).

[12]D. P. Landau, S.-H. Tsai, and M. Exler, American Journal of Physics **72**, 1294–1302 (2004).

[13]R. Evans, Advances in Physics **28**, 143–200 (1979).

[14]R. Evans, *Density functional theory for inhomogenous fluids, Simple fluids in equilibrium*, Lecture notes, Kazimierz Dolny, 2009.

[15]E. T. Jaynes, Physical Review **106**, 620–630 (1957).

[16]T. J. H. Vlugt, J. P. J. M. van der Eerden, M. Dijkstra, B. Smit, and D. Frenkel, *Introduction to Molecular Simulation and Statistical Thermodynamics* (Delft, The Netherlands, 2008).

[17]L. Rowley, D. Nicholson, and N. Parsonage, Journal of Computational Physics **17**, 401–414 (1975).

[18]R. Roth, *Introduction to Density Functional Theory of Classical Systems: Theory and Application*, Lecture notes, Fukuoka and Tübingen, 2006 and 2013.

[19] R. Evans, M. Oettel, R. Roth, and G. Kahl, Journal of Physics: Condensed Matter **28**, 240401 (2016).

[20] J. K. Percus, Journal of Statistical Physics **15**, 505–511 (1976).

[21] E. Kierlik and M. L. Rosinberg, Physical Review A **42**, 3382–3387 (1990).

[22] J. F. Lutsko and J. Lam, Physical Review E **98**, 012604 (2018).

[23] Y. Rosenfeld, Physical Review Letters **63**, 980–983 (1989).

[24] R. Roth, R. Evans, A. Lang, and G. Kahl, Journal of Physics: Condensed Matter **14**, 12063–12078 (2002).

[25] H. Hansen-Goos and R. Roth, Journal of Physics: Condensed Matter **18**, 8413–8425 (2006).

[26] M. Schmidt, Physical Review E **84**, 051203 (2011).

[27] H. Tetrode, Annalen der Physik **343**, 434–442 (1912).

[28] G. Leithall and M. Schmidt, Physical Review E **83**, 021201 (2011).

[29] M. Levesque, R. Vuilleumier, and D. Borgis, The Journal of Chemical Physics **137**, 034115 (2012).

[30] T. Eckert, N. C. X. Stuhlmüller, F. Sammüller, and M. Schmidt, “Fluctuations in inhomogeneous liquids”, to be published, 2020.

[31] R. Evans and M. C. Stewart, Journal of Physics: Condensed Matter **27**, 194111 (2014).

[32] R. Evans and N. B. Wilding, Phys. Rev. Lett. 115, 016103 (2015) (2015).

[33] B. Chacko, R. Evans, and A. J. Archer, The Journal of Chemical Physics **146**, 124703 (2017).

[34] E. Xi, R. C. Remsing, and A. J. Patel, Journal of Chemical Theory and Computation **12**, 706–713 (2016).

[35] T. Eckert, “The role of fluctuation profiles in the theory of inhomogeneous fluids”, MA thesis (Universität Bayreuth, Bayreuth, 2020).

[36] N. Stuhlmüller, “Local susceptibilities in Gaussian and Lennard-Jones fluids”, MA thesis (Universität Bayreuth, Bayreuth, 2020).

[37] A. P. Lyubartsev, A. A. Martsinovski, S. V. Shevkunov, and P. N. Vorontsov-Velyaminov, The Journal of Chemical Physics **96**, 1776–1783 (1992).

[38] H. Do, J. D. Hirst, and R. J. Wheatley, The Journal of Chemical Physics **135**, 174105 (2011).

[39] N. F. G. Martin and J. W. England, *Mathematical Theory of Entropy*, Vol. 12 (Cambridge University Press, Dec. 1984).

Erklärung der Selbstständigkeit

Hiermit erkläre ich, dass ich die vorliegende Masterarbeit selbstständig verfasst und dazu keine anderen als die angegebenen Hilfsmittel verwendet habe. Insbesondere sind die aus fremden Quellen direkt oder indirekt übernommenen Stellen als solche kenntlich gemacht.

Die Arbeit wurde bisher in gleicher oder ähnlicher Form keiner anderen Prüfungsbehörde vorgelegt.

Ort, Datum

Florian Sammüller